ABSTRACT

Title of Dissertation: MOLECULAR MASS MANIPULATION ENABLED BY GRAPHENE BASED NANOSTRUCTURES

Yinjun Huang, Doctor of Philosophy, 2016

Dissertation directed by: Associate Professor Dr. Teng Li Department of Mechanical Engineering

The surge of interest in graphene, as epitomized by the Nobel Prize in Physics in 2010, is attributed to its extraordinary properties. Graphene is ultrathin, mechanically tough, and has amendable surface chemistry. These features make graphene and graphene based nanostructure an ideal candidate for the use of molecular mass manipulation. The controllable and programmable molecular mass manipulation is crucial in enabling future graphene based applications, however is challenging to achieve. This dissertation studies several aspects in molecular mass manipulation including mass transportation, patterning and storage.

For molecular mass transportation, two methods based on carbon nanoscroll are demonstrated to be effective. They are torsional buckling instability assisted

transportation and surface energy induced radial shrinkage. To achieve a more controllable transportation, a fundamental law of direction transport of molecular mass by straining basal graphene is studied.

For molecular mass patterning, we reveal a barrier effect of line defects in graphene, which can enable molecular confining and patterning in a domain of desirable geometry. Such a strategy makes controllable patterning feasible for various types of molecules.

For molecular mass storage, we propose a novel partially hydrogenated bilayer graphene structure which has large capacity for mass uptake. Also the mass release can be achieved by simply stretching the structure. Therefore the mass uptake and release is reversible. This kind of structure is crucial in enabling hydrogen fuel based technology.

Lastly, spontaneous nanofluidic channel formation enabled by patterned hydrogenation is studied. This novel strategy enables programmable channel formation with pre-defined complex geometry.

MOLECULAR MASS MANIPULATION ENABLED BY GRAPHENE BASED NANOSTRUCTURES

By

Yinjun Huang

Dissertation submitted to the Faculty of the Graduate School of the
University of Maryland, College Park, in partial fulfillment
of the requirements for the degree of
Doctor of Philosophy
2016

Advisory Committee:
Associate Professor Teng Li, Chair
Professor Abhijit Dasgupta
Assistant Professor Liangbing Hu
Assistant Professor Yifei Mo
Associate Professor Yuhuang Wang, Dean's Representative

© Copyright by

Yinjun Huang

2016

Table of Contents

CHAPTER 1: INTRODUCTION 1

1.1. Background 1

1.2. Properties of Graphene 2

1.2.1. Single atom thickness 3

1.2.2. Mechanical properties 3

1.2.3. Band structure 3

1.2.4. Electron mobility and electronic conductivity 4

1.2.5. Negative coefficient of thermal expansion 4

1.2.6. Amendable surface chemistry 4

1.3. Molecular Mass Manipulation 4

1.4. Dissertation Layout 6

CHAPTER 2: MOLECULAR MASS TRANSPORTATION VIA CARBON NANOSCROLLS ..9

2.1. Background 9

2.2. Adsorption of Hydrogen into a CNS 12

2.3. Molecular Hydrogen Transport Enabled by Torsional Buckling of the CNS 13

2.3.1. Simulation model and results 13

2.3.2. Discussion 18

2.4. Molecular Hydrogen Transportation Enabled by Surface Energy Induced Radial Shrinking of a CNS 19

2.4.1. Energetics of CNS 19

2.4.2. Simulation model and results 21

2.5. Summary 24

CHAPTER 3: DIRECTIONAL TRANSPORT OF MOLECULAR MASS ON GRAPHENE BY STRAINING 26

3.1. Background 26

3.2. Theoretical Framework of Net Transport Force on Molecular Mass Induced by a Strain Gradient in Graphene 28

3.2.1. A single atom model 28

3.2.2. Validation by simulation 31

3.3. Directional Transport of Molecular Mass on Graphene by Straining....32

3.4. Potential Application....38

3.5. Summary and Discussions....40

CHAPTER 4: LINE DEFECTS GUIDED MOLECULAR PATTERNING ON GRAPHENE....41

4.1. Background 41

4.2. Theoretical Foundation....43

4.3. Simulation Results....46

4.3.1. C_{60} molecules patterned in square shaped domain 46

4.3.2. C_{60} molecules patterned in domains of arbitrary geometries....50

4.3.3. C_{60} molecules patterned in large domain....51

4.4. Summary 52

CHAPTER 5: HYDROGENATION ENABLED NANOSTRUCTURE FOR MOLECULAR MASS MANIPULATION....54

5.1. Hydrogenation of Graphene 55

5.2. Molecular Mass Storage and Release Enabled by Hydrogenated Bilayer Graphene Structure…… ……..56

5.2.1. Background 56

5.2.2. Hydrogenation enabled graphene bilayer opening 58

5.2.3. Hydrogen storage 61

5.2.4. Mass release by displacement loading 62

5.3. Hydrogenation Enabled Nanofluidic Channel....64

5.3.1. Background 64
5.3.2. Hydrogenation enabled channel formation 66
5.3.3. Channel with junction 67
5.3.4. Channel network 69
5.3.5. Channel with changing cross section area 70
5.4. Summary 73
CHAPTER 6: SUMMARY AND FUTURE WORK 75
6.1. Summery and Concluding Remarks 75
6.2. Future Work 77
6.2.1. Straining induced vdW force change and its effect on mass transportation 77
6.2.2. Generation of strain gradient in graphene by experiment method 77
BIBLIOGRAPHY 79

List of Figures

Figure 1.1 Graphene is the building block of graphitic allotropes [1]..... 1
Figure 2.1 The structure of CNS. (a) End view; (b) Side view 11
Figure 2.2 (a). Perspective view of a CNS (green) immersed in a hydrogen reservoir. (b)-(d). Sequential snapshots of the end view (top) and side view (bottom) of the CNS with hydrogen physisorption at 50 ps, 150 ps and 250 ps, respectively. For visual clarity, hydrogen molecules outside of the CNS are not shown. 13
Figure 2.3 (a). Resultant torque as a function of twisting angle per unit length for a 4-layer CNS (solid line) and a 4-layer multi-wall carbon nanotube (MWCNT) (dashed line), respectively. Insets 1 and 2 show the deformed shapes of the 4- layer MWCNT at a twisting angle of 0.049 nm^{-1} (right after onset of buckling) and a post-buckling twisting angle of 0.07 nm^{-1}, respectively. (b) Resultant torque as a function of twisting angle per unit length for CNSs (solid lines) and MWCNTs (dashed lines) of various diameters. [51]..... 15
Figure 2.4 (a) Resultant torque as a function of twisting angle per unit length for the CNS immersed in a hydrogen reservoir. The change of slope indicates the onset of torsional buckling. (b) Percentage of hydrogen molecules remaining inside the CNS as a function of twisting angle per unit length. After the occurrence of torsional buckling, the collapse of the CNS squeezes more adsorbed hydrogen molecules out of the CNS, as indicated by the change of slope of the curve. (c)-(e) The side and end views of the CNS (green) and the hydrogen molecules (red) initially adsorbed inside the CNS inner core at the onset of torsional buckling (0.03 rad/nm) and at a twisting angle of 0.105 rad/nm and 0.17 rad/nm, respectively. For visual clarity, the hydrogen molecules initially outside of the CNS are not shown. 16
Figure 2.5 Percentage of hydrogen molecules remaining inside the CNS as a function of twisting angle per unit length, for four different loading rates. 18
Figure 2.6 Change in total energy during scrolling of graphene to make a CNS. The strain energy and the van der Waals energies are shown in the inset graph [36] 21

Figure 2.7 Sequential snapshots of the hydrogen molecules (red) initially adsorbed inside a CNS (green) being squeezed out of the CNS due to the radial shrinkage of the CNS driven by a sudden increase of the surface energy of the basal graphene. For visual clarity, the hydrogen molecules initially outside of the CNS are not shown. .. 23
Figure 2.8(a) Percentage of hydrogen molecules remaining inside the CNS as a function of simulation time, for four different tuning factors of surface energy of the basal graphene. (b) End view and resultant inner core diameter of the CNS at the end of the simulation for each case. For visual clarity, hydrogen molecules are not shown. 24
Figure 3.1(a) Schematic showing that a net force $FvdW$ acting on an atom (red dot) positioned above on a basal graphene subject to a strain gradient points to the decreasing strain direction. (b) $FvdW$ as a function of position along *y* direction for various lengths of basal graphene and strain gradients. (c) Molecular mechanics model of a round graphene flake on a basal graphene subject to a strain gradient to compute the overall net force $Ftransport$ acting on the graphene flake, which is plotted as a function of position along *y* direction for various strain gradients (d). ... 30
Figure 3.2 Snapshots of MD simulations of programmable directional transport of a round graphene flake (green) on a graphene nanoribbon (GNR) by controlling the strain gradient in the GNR. 34
Figure 3.3 MD simulations on directional transport of a CNT on a GNR subject to a strain gradient. (a) Schematic of simulation model and applied strain gradient. (b) Snapshots of the transport process of the CNT toward decreasing strain direction. Several rows of carbon atoms in the CNT are shaded in blue to reveal the CNT rolling on the GNR (see Supplementary Materials for a simulation video), resulting from a net torque due to unbalanced vdW attraction in vertical direction acting on the CNT (c). (d-g) Transport distance of the CNT as a function of simulation time for various $emax$ and combinations of chirality of the CNT (by its edges) and the GNR (by its longer edges). 36

Figure 3.4 MD simulations of the directional motion of various molecular cargos on a GNR subject to a strain gradient. (a) A gold nanoparticle (purple) on a round graphene flake (green). (b) Four C_{60} molecules (purple) housed in a CNT (green)... 37
Figure 3.5 MD simulations on the pumping effect in a graphene bilayer nanochannel induced by a strain gradient. (a) Top view and side view of a C_{60} molecule located near the top end of a graphene bilayer nanochannel subject to a strain gradient. The maximum applied strain is 15%. (b) The trajectory of the C_{60} molecule in the graphene bilayer nanochannel. For visual clarity, the top graphene layer is not shown. 39
Figure 4.1 (a) A 3 Å-wide open slit is introduced in a graphene monolayer by knocking off a row of carbon atoms and is composed of two zigzag edges. A C_{60} molecule is placed near the slit with an out-of-plane distance of 8 Å to the graphene sheet. (b) Net in-plane vdW force acting on the C_{60} as a function of the distance of C_{60} to the open slit. Dashed lines mark the location of the edges of the open slit..... 46
Figure 4.2 (a) Initial configuration of the simulation, nine C60s are randomly distributed in the square-shaped domain enclosed by four slits. (b) At 7 ps, five of nine C60s start to cluster into a triangular pattern. (c) At 87 ps, all nine C60s self-assemble into a larger cluster with a triangular lattice. (d) Three more C60s are added to the existing system. (e) Two of the three newly added C_{60}s are self-assemble into the cluster. (f) All the 12 C_{60}s form a larger cluster with triangular lattice. 48
Figure 4.3 More C_{60}s (shown in blue color) are continuously added into the square-shaped domain (left column) step by step, which can readily self-assemble into the existing cluster (right column) in a well-defined triangular lattice. Eventually the squared domain can accommodate 23 C_{60}s. 49
Figure 4.4 Domains of different shapes, e.g., (a) square, (b) triangular, (c) circular, and (d) hexagonal, can be generated in graphene to pattern C_{60}s into a cluster of designated geometry. 51

Figure 4.5 A large square-shaped confining domain with side length of 10 nm is generated in a graphene sheet, which can accommodate 90 C_{60}s densely packed into a triangular lattice as a giant molecular cluster. 52
Figure 5.1 Side view and top view of the computation model. Basal graphene sheets have a length of 300 Å and a width 30 Å, they are both single-sided hydrogenated for a length of 100 Å. Red denotes the hydrogen atoms. 59
Figure 5.2 Sequential snapshots of the bilayer opening process enabled by hydrogenation. Driven by the hydrogenation induced local lattice distortion, the hydrogenated portions detach from each other and form a tunnel shape. 60
Figure 5.3 Tunnel shape and area as a function of hydrogenation length. 61
Figure 5.4 A complete table of total hydrogen atoms stored in the bilayer structure as a function of hydrogenation width and the delamination length. 62
Figure 5.5 Number of hydrogen molecules remaining inside the bilayer structure as a function of the displacement of the two ends. At the end of the loading, 82.3% of the hydrogen molecules initially adsorbed are squeezed out of the bilayer 64
Figure 5.6 Side view and top view of the computation model. Basal graphene sheet has a length of 100 Å and a width of 110 Å. The single-sided hydrogenated strip has a width of 30 Å. Red denotes the hydrogen atoms. 66
Figure 5.7 Hydrogenated strip detaches from supporting layer and form a channel. . 66
Figure 5.8 Top view of the computation model. Basal graphene sheet has a side length of 185 Å. The two single-sided hydrogenated strip has a width of 30 Å. Red denotes the hydrogen atoms. 68
Figure 5.9 Channel with junction spontaneously formed after biaxial compression enabled by two stripes of hydrogenation. 69
Figure 5.10 Hydrogen molecules flow in the channel network. Hydrogen flux is provided from the channel entrance on the right side. For visual clarity, the bottom layer is not shown here. 70
Figure 5.11 Top view of the computation model. Red denotes hydrogen atoms. 71

Figure 5.12 (a) Top view and (b) side view of the funnel shaped tunnel. 72
Figure 5.13 Illustration of the selective feature of the funnel shaped channel. Initially a mixture of hydrogen atoms and a C_{60} are placed inside the channel. A virtual wall is used to push them towards the smaller end. As they arrive near the end, the hydrogen molecules are pushed out of the channel while the C_{60} remains inside. 73

Chapter 1: Introduction

1.1. Background

Graphene is a monolayer of carbon atoms tightly packed into a two-dimensional (2D) honeycomb lattice with an inter-atomic distance approximately 0.142nm. It serves as a basic building block for graphitic materials of other dimensionalities. For example, graphene can be wrapped up into fullerenes (0D), rolled into nanotubes (1D) or stacked into graphite (3D) (Figure 1.1) [1].

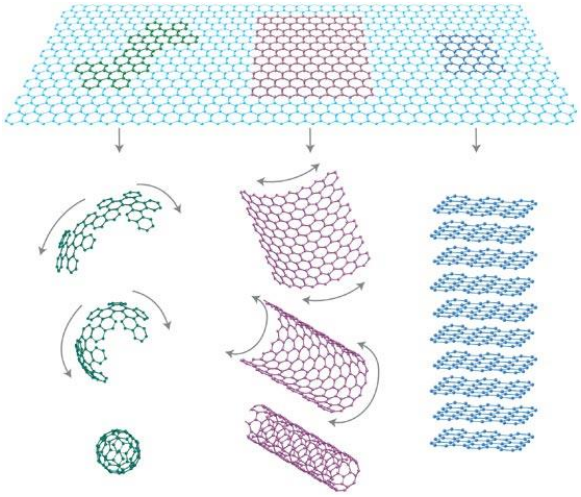

Figure 1.1 Graphene is the building block of graphitic allotropes [1]

People once believed that perfect two-dimensional crystals were not thermodynamically stable since thermal fluctuation tends to destroy the long-range order of atoms when the 2D film has only a few atomic layers thick [2]. This misconception has not been clarified until in 2004 that the researchers from University of Manchester obtained monolayer graphene on silicon substrate by using scotch tape to peel off thin layers from bulk graphite, which simply consists of many

graphene sheets stacking together by weak inter-molecular van der Waals force [3]. This simple and straightforward procedure is called mechanical exfoliation. After the exfoliated flakes were transferred on to a silicon substrate, further measurements showed that the monolayer graphene sheets are continuous and exhibit high crystal quality. Later on, other groups also confirmed the existence of free-standing graphene [4]. The discovery of graphene is groundbreaking, and the 2010 Nobel Prize in Physics has been awarded to Professors Andre Geim and Konstantin Novoselov from the University of Manchester who had made great contribution for it [5].

The idea of mechanical exfoliation to obtain graphene is very straightforward, however, its limitation is that the graphene size is quite limited and also the output is low [6]. Researches have been conducted on massive production of graphene. Chemical vapor deposition on metal substrate [7-10], graphite oxide reduction [11], and epitaxial growth on silicon carbide substrate [12] have been effective methods to fabricate graphene in large scale. With these progresses on fabrication techniques, now people are able to fabricate graphene with size as large as several square feet. The large scale production of graphene with lower cost will surely further enable its potential application in various aspects.

1.2. Properties of Graphene

Graphene has exceptional electronic and mechanical properties as summarized below, many of which result from graphene's unique two dimensional planar structure.

1.2.1. Single atom thickness

Graphene has only a single atom thick, which is the thinnest material in the world. This property makes graphene an ideal membrane for separation of chemical mixtures because its infinitesimal thickness promises ultimate permeation [13].

1.2.2. Mechanical properties

While being the thinnest material in the world, graphene is the strongest. It has the young's modulus of ~1 TPa and the tensile strength of 130 GPa, which is 200 times larger than that of steel [14]. The fracture strain of graphene is measured to be as large as 25% [15], which means it has a great ductility. And atomistic simulations show that the chirality of graphene plays a role in fracture: the nominal strain of fracture is considerably lower for the uniaxial tensile loading along armchair direction than along zigzag direction [16].

1.2.3. Band structure

While the intrinsic graphene is a semi-metal or zero-gap semiconductor [17], the band structure of graphene is highly tunable. For instance, narrow graphene nanoribbon will have a completely different band structure [16,17]. Experiment has demonstrated that a 200 meV energy gap can be opened by reducing the graphene nanoribbon width to 15 nm [18]. For bilayer graphene, the energy gap can be continuously tuned by two gate voltages up to 250 meV [19].

1.2.4. Electron mobility and electronic conductivity

It's reported that the electron mobility of graphene is in excess of 15,000 $cm^2V^{-1}s^{-1}$, which is 100 times larger than silicon [17]. Graphene also has the lowest resistivity at room temperature, which is 10^{-6} Ω·cm and less than that of silver [18].

1.2.5. Negative coefficient of thermal expansion

Unlike most materials that expand in volume when the temperature increases, interestingly graphene shrinks when heated up. Therefore the coefficient of thermal expansion (CTE) of graphene is negative and measured to be $\sim -7 \times 10^{-6}\ K^{-1}$ at room temperature [15].

1.2.6. Amendable surface chemistry

Graphene, as a two-dimensional material, exposes its entire volume to its surrounding, which leads to a highly amenable surface chemistry. Pristine graphene can be functionalized by bonding with foreign atoms, molecules and functional groups on its surface [21-27]. This serves a potential method to modify the morphology of graphene and achieve novel graphene based nanostructures.

1.3. Molecular Mass Manipulation

The manipulation of matter on an atomic or molecular scale reveals many interesting phenomenon and is very important in nanotechnology. It's the key enabling technology in novel molecular devices and machines. For example, people can control the motion of molecule on a metal surface by electronic and vibrational excitation [28]; it's also reported that an artificial nanofabricated motor which is

made of one short carbon nanotube moving relative to another coaxial nanotube can be actuated by imposing a thermal gradient along the inner nanotube. A cargo is attached to an ablated outer wall of a multi-walled carbon nanotube that can rotate and/or translate along the inner nanotube [29]. The precise control of molecular mass will find many potential applications such as chemical reaction control, drug delivery, and nano-molecular mechanical systems. The challenge here is to manipulate molecular mass in a controllable, programmable fashion rather than molecules acting as passive elements.

Graphene and graphene based novel nanostructures are ideal platforms for molecular mass manipulation, considering its extraordinary properties. For example, its high deformability and strength makes it possible to exert mechanical loading as a way to control its morphology. Also graphene has amendable surface chemistry, which will give rise to an array of unconventional nanostructures. Therefore many novel derivative structures can be designed to serve the molecular mass manipulation purpose.

Therefore, in this dissertation, we will study graphene and graphene based nanostructures as a medium to achieve molecular mass manipulation in a controllable and programmable fashion. We will cover several aspects of molecular mass manipulation, including transportation, patterning, storage and release. The structures involved will include graphene, carbon nanoscrolls which is formed by rolling a basal graphene sheet, and bilayer graphene.

1.4. Dissertation Layout

To address the research objectives outlined above, the rest of the dissertation is organized as follows.

In Chapter 2, we discuss the molecular mass transportation via carbon nanoscrolls. The open topology of a carbon nanoscroll inspires potential applications such as high capacity hydrogen storage. One crucial problem that remains largely unexplored is how to shuttle the hydrogen molecules adsorbed inside the CNSs. Given the fundamental structural difference between carbon nanotube and carbon nanoscroll, two effective transportation mechanisms of hydrogen molecules enabled by the torsional buckling instability of a CNS and the surface energy induced radial shrinkage of a CNS are revealed by using molecular dynamics simulations.

Chapter 3 focuses on the directional transport of molecular mass on graphene sheet which is a more controllable transportation but often challenging to achieve. We combine theoretical analysis and molecular simulations to demonstrate a facile mechanism of directional transport of molecular mass on graphene by a simple stretch. We reveal that stretch-induced strain gradient in graphene leads to a net transport force that is sufficient to drive molecular cargo on the graphene in a directional fashion. The large elastic deformability of graphene and the van Der Waals nature of the transport force allow for programmable directional transport of various types of molecular cargo.

In Chapter 4, molecular patterning and confining is studied. To achieve molecular self-assembly in domains of desirable geometries, we reveal a barrier effect of line defects (e.g., open slits) in graphene, which can potentially enable molecular confining and patterning in a domain of desirable geometry. Using molecular dynamics simulations, we demonstrate that fullerene molecules can be readily patterned into a stable cluster of various shapes and sizes. Such a strategy is also expected to be applicable to pattern various types of molecules that interact with graphene via van der Waals force.

In Chapter 5, novel hydrogenation enabled structures are designed to serve specific molecular mass manipulation function. Firstly, molecular mass storage and release enabled by hydrogenated bilayer graphene structure is investigated. A key step for the development of a reliable hydrogen-based technology requires solving the issue of storage and transport of hydrogen. A novel structure which allows reversible mass uptake and release thus is desirable. In this Chapter, using molecular dynamics simulation, we show a partially hydrogenated bilayer graphene structure will serve this end. Simulation results show this kind of structure can adopt a tunnel shape which provides space for hydrogen storage. To release the hydrogen, a displacement loading at two ends can lead to a transportation efficiency as high as 82.3%. Following this idea, hydrogenation assisted nanofluidic channel formation is also studied. While the existing nanofluidic channels only have a relatively simple geometry, we proposed this novel strategy of patterning hydrogenation stripes on graphene sheet to have complex nanofluidic channels spontaneously formed.

Chapter 6, the major findings and contributions of the dissertation are summarized and discussed, followed by an outlook of future work.

Chapter 2: Molecular Mass Transportation via Carbon Nanoscrolls

The open topology of a carbon nanoscroll (CNS) inspires potential applications such as high capacity hydrogen storage. Enthusiasm for this promising application aside, one crucial problem that remains largely unexplored is how to shuttle the hydrogen molecules adsorbed inside CNSs. In this Chapter, using molecular dynamics simulations, we demonstrate two effective transportation mechanisms of hydrogen molecules. In Section 2.3, the torsional buckling instability of a CNS is studied and proved to be a feasible method to transport hydrogens. In Section 2.4, the surface energy induced radial shrinkage of a CNS is investigated. Results will be discussed in Section 2.5. As these two mechanisms essentially rely on the non-bonded interactions between the hydrogen molecules and the CNS, it is expected that similar mechanisms could be applicable to the transportation of molecular mass of other types, such as water molecules, DNAs, fullerenes and nanoparticles.

2.1. Background

A carbon nanoscroll (CNS) is formed by rolling up a graphene sheet into a spiral nanostructure. A CNS is topologically open thus its core size can be tuned by relative sliding between adjacent layers. By contrast, a carbon nanotube (CNT) is topologically closed; therefore the radius of a CNT can only be modestly increased by stretching and deflecting the carbon-carbon (C-C) covalent bonds. The highly tunable

structure of CNSs has inspired research efforts to explore their potential applications [30-40]. Especially, previous studies have found that CNSs have great potential for hydrogen storage [31-34]. Galvao *et al.* predicted it by classical grand-canonical Monto Carlo simulation that hydrogen molecules can be absorbed in the internal cavity as well as on the external surface of the scroll, reaching a 2.5% weight percentage which is higher than the values obtained for crystallographically packed single walled carbon nanotubes at same condition [32]. In addition, the spiral structure of a CNS can be further opened by alkali doping thus allows the CNS to accommodate more hydrogen than a CNT [34]. Froudakis *et al.* has used a multiscale theoretical approach to show that while pure carbon nanoscrolls cannot accumulate hydrogen because the interlayer distance is too small, alkali doping opens of the spiral structure to approximately 7 Å comparing to the original 3.4 Å. In this way, a 3% weight percentage hydrogen storage can be achieved even at ambient temperature and pressure [34].

Enthusiasm for this promising application aside, one crucial problem that remains largely unexplored is how to make effective molecular mass transportation through CNSs. For example, it remains elusive how to shuttle the hydrogen molecules adsorbed inside CNSs. It is desirable to explore an effective molecular mass transportation mechanism to enable the future application of CNS-based hydrogen storage.

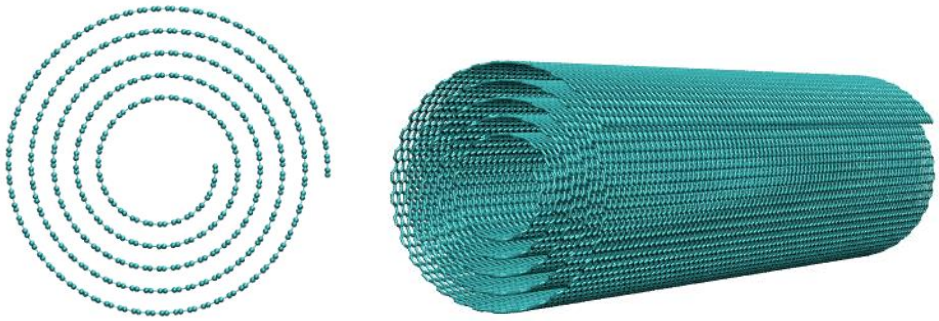

Figure 2.1 The structure of CNS. (a) End view; (b) Side view

In the area of mass transportation, a lot of studies have been done on CNT in recent years [41-45]. A few approaches have been demonstrated experimentally or theoretically. For example, Wang *et al.* showed by molecular dynamics simulation that various species of molecules (e.g., hydrogen, helium atoms and DNA) can be transported using a CNT in torsion, which is a result of the van der Waals effect through the propagation of the kink initiated at the onset of the tube torsional buckling [41,42]; They also showed that transportation of water molecules can be realized by a CNT pump with a small portion of initially twisted wall [43]; Hassanein *et al.* revealed a "nanopumping" effect: by Rayleigh travelling waves on the tube surface, gas flow can be conducted inside CNT as the friction between the gas particles and nanotube walls serving as driving force [45].

Inspired by these research progresses and taking into account the open and highly tunable structure of CNSs, we use molecular dynamics (MD) simulations to investigate two effective mechanisms of molecular hydrogen transportation enabled by (a) the torsional buckling instability of CNSs and (b) surface energy induced radial shrinking of CNSs.

2.2. Adsorption of Hydrogen into a CNS

We first use MD simulation to demonstrate the physisorption of hydrogen molecules into a CNS. The CNS in the MD simulation has a length of 8 nm and inner core diameter of 2 nm (perspective view shown in Figure 2.1.a). The second-generation reactive empirical bond order potential [46] and 12-6 Lennard-Jones potential [47] are adopted to describe the C-C covalent interaction and van der Waals (vdW) force, respectively. The CNS is initially immersed in a hydrogen reservoir to achieve hydrogen adsorption (Figure 2.1.a). To simulate the hydrogen physisorption on the CNS, the hydrogen-carbon vdW interaction is also described by 12-6 Lennard-Jones potential $V_{CH}(r) = 4\varepsilon_{CH}(\frac{\sigma_{CH}^{12}}{r^{12}} - \frac{\sigma_{CH}^{6}}{r^{6}})$, where r is the hydrogen-carbon atomic pair distance, $\varepsilon_{CH} = 2.998 \times 10^{-3} eV$ and $\sigma_{CH} = 3.18\, nm$ [48]. Note that chemisorption of hydrogen molecules on the CNS could also occur [49], which can potentially lead to a higher hydrogen storage capacity, while only physisorption is considered in this study. The simulation is carried out using Large-scale Atomic/Molecular Massively Parallel Simulator (LAMMPS) [50] with Canonical Ensemble at a temperature of 70K and a time step of 0.001 ps. Driven by the concentration gradient, hydrogen molecules are shown to enter the CNS structure and then be physically adsorbed inside the CNS due to the vdW adhesion. Figure 2.1.b-2.1.d shows sequential snapshots of the end view of the CNS with hydrogen physisorption at 50 ps, 150 ps and 250 ps, respectively. After about 300 ps, the hydrogen physisorption into the CNS reaches equilibrium, with 572 hydrogen molecules adsorbed and adhered to the inner walls of CNS, corresponding to a

gravimetric hydrogen uptake of 1.56 wt%. It is also interesting that hydrogen molecules adsorbed inside the CNS core form a spiral structure in extension of the CNS structure, similar to the previous findings of water molecules confined inside a CNS core [36].

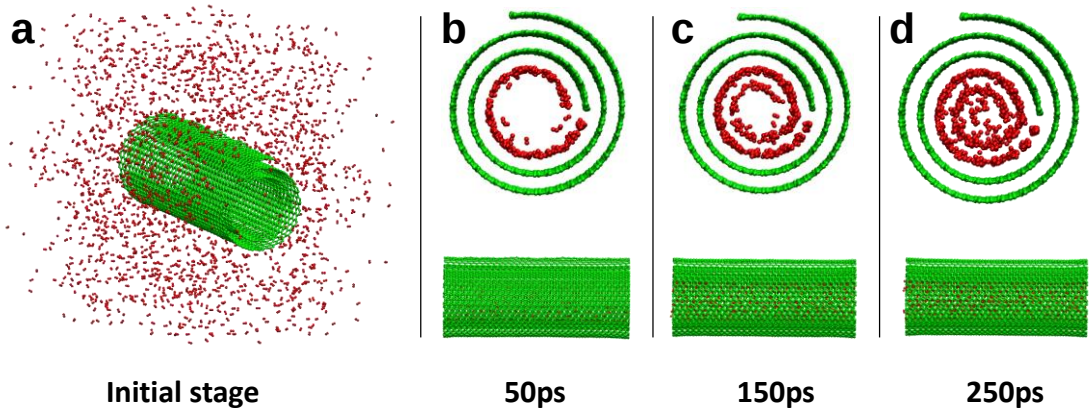

Figure 2.2 (a). Perspective view of a CNS (green) immersed in a hydrogen reservoir. (b)-(d). Sequential snapshots of the end view (top) and side view (bottom) of the CNS with hydrogen physisorption at 50 ps, 150 ps and 250 ps, respectively. For visual clarity, hydrogen molecules outside of the CNS are not shown.

2.3. Molecular Hydrogen Transport Enabled by Torsional Buckling of the CNS

2.3.1. Simulation model and results

Recent studies of the buckling instability under mechanical loads of CNSs [51] reveal that the torsional buckling behavior of a CNS is distinct from that of a CNT of similar size due to their fundamental difference in their topologies. Intuitively, a CNS is a one-layer spiral structure, in which a local perturbation may

propagate through the C-C bonds network in the basal graphene sheet and thus the overall structure is impacted. However, for a multi-walled CNT, local deformation in one carbon nanotube can hardly affect adjacent layers via very weak inter-layer van der Waals force. Another important structural feature of CNS that is very distinct from CNT is that CNS has two free edges in axial direction, one along inner core and another along outer surface respectively. Studies have showed that these free edges have intrinsic compressive edge stress and have a tendency to wrinkle at equilibrium state. This kind of wrinkle will serve as an intrinsic geometric imperfection to initiate buckling instability. For these reasons, the critical buckling loading of a CNS is much lower than that of a MWCNT of similar diameter as figure2.3 shows. Furthermore, it can be seen from the figure that the torsional buckling of a CNS occurs in a much more gradual manner compared to the abrupt buckling process of a CNT under torsion. Such a feature is desirable to achieve a smooth molecular mass transportation. In this section, we demonstrate molecular hydrogen transportation enabled by torsional buckling of a CNS.

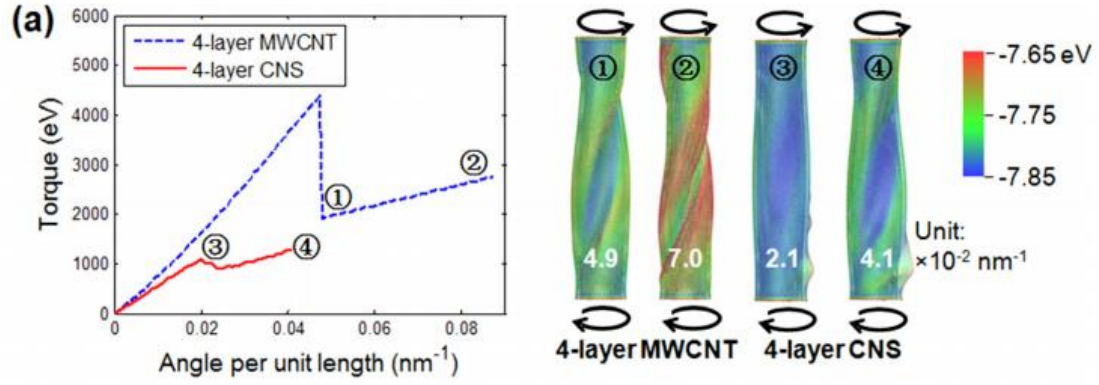

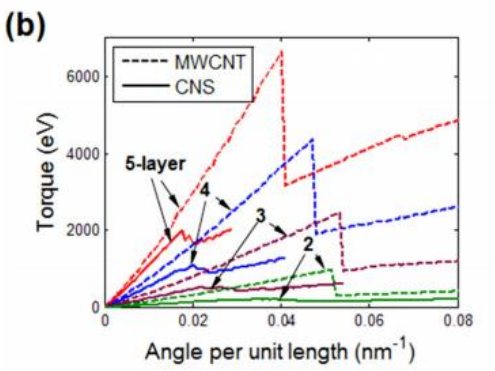

Figure 2.3 (a). Resultant torque as a function of twisting angle per unit length for a 4-layer CNS (solid line) and a 4-layer multi-wall carbon nanotube (MWCNT) (dashed line), respectively. Insets 1 and 2 show the deformed shapes of the 4- layer MWCNT at a twisting angle of 0.049 nm^{-1} (right after onset of buckling) and a post-buckling twisting angle of 0.07 nm^{-1}, respectively. (b) Resultant torque as a function of twisting angle per unit length for CNSs (solid lines) and MWCNTs (dashed lines) of various diameters. [51]

To achieve the transportation of the adsorbed hydrogen molecules through the CNS, a torsional deformation along the length direction up to 0.17 rad/nm is gradually applied to the CNS by fixing the left end of and twisting its right end with a loading rate of 5.45×10^{-4} rad/nm/ps. The torsional buckling of the CNS and the associated transportation process of hydrogen adsorbed in the CNS are illustrated in Figure 2.4.

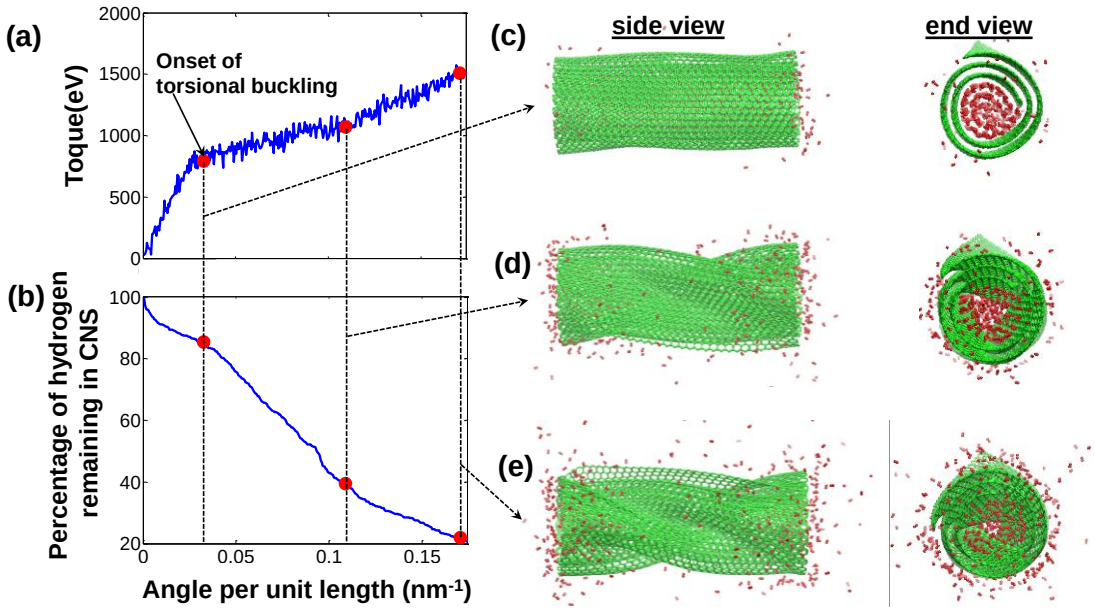

Figure 2.4 (a) Resultant torque as a function of twisting angle per unit length for the CNS immersed in a hydrogen reservoir. The change of slope indicates the onset of torsional buckling. (b) Percentage of hydrogen molecules remaining inside the CNS as a function of twisting angle per unit length. After the occurrence of torsional buckling, the collapse of the CNS squeezes more adsorbed hydrogen molecules out of the CNS, as indicated by the change of slope of the curve. (c)-(e) The side and end views of the CNS (green) and the hydrogen molecules (red) initially adsorbed inside the CNS inner core at the onset of torsional buckling (0.03 rad/nm) and at a twisting angle of 0.105 rad/nm and 0.17 rad/nm, respectively. For visual clarity, the hydrogen molecules initially outside of the CNS are not shown.

The evolution of the amount of the adsorbed hydrogen molecules remaining inside the CNS is presented as a function of the applied torsional deformation (Figure 2.4b). Initial deformation causes the tightening of the CNS, reducing the cross section area, which in turn imposes a stronger repulsive vdW forces on the hydrogen molecules. As a result, some hydrogen molecules are pushed out of the CNS. Upon

further applying the torsional loading, the CNS buckles when the deformation reaches 0.031 rad/nm. At this stage, 14.5% of the adsorbed hydrogen molecules are squeezed out of the CNS. Note that the onset of torsional buckling of the CNS (Figure 2.4a) is much more gradual than that of a CNT of similar size, which is often indicated by a sharp drop of the resultant torque at the onset of buckling [51]. As torsional buckling develops, much more adsorbed hydrogen molecules are transported through the CNS as indicated by a steeper slope of the curve in Figure 2.4 beyond the onset of buckling. At the end of the loading, 79.4% of the hydrogen molecules initially adsorbed inside the CNS are squeezed out of the CNS, suggesting the high efficacy of the molecular transport by torsional buckling instability of the CNS. In this simulation, a relatively short CNS is used, to which torsion may be challenging to apply in real situation. A long CNS, however, buckles more easily under torsion, and the hydrogen inside can eventually be pushed out as the deformation of the CNS wall continues to develop. Therefore the hydrogen transport mechanism demonstrated here still holds. A bundle of CNSs subject to torsion can also lead to the molecular mass transport in a similar fashion but could be more realistic to achieve in experiment.

To investigate the effect of loading rate on the efficacy of torsional buckling enabled molecular mass transportation, we performed MD simulations at four different loading rates of 2.725×10^{-4} rad/nm/ps, 5.45×10^{-4} rad/nm/ps, 1.09×10^{-3} rad/nm/ps, and 2.18×10^{-3} rad/nm/ps, respectively. Figure 2.5 plots the percentage of hydrogen molecules remaining inside the CNS as a function of twisting angle per unit length for these four cases. It's shown that the total amount of hydrogen molecules squeezed out of the CNS increases modestly as the loading rate gets lower.

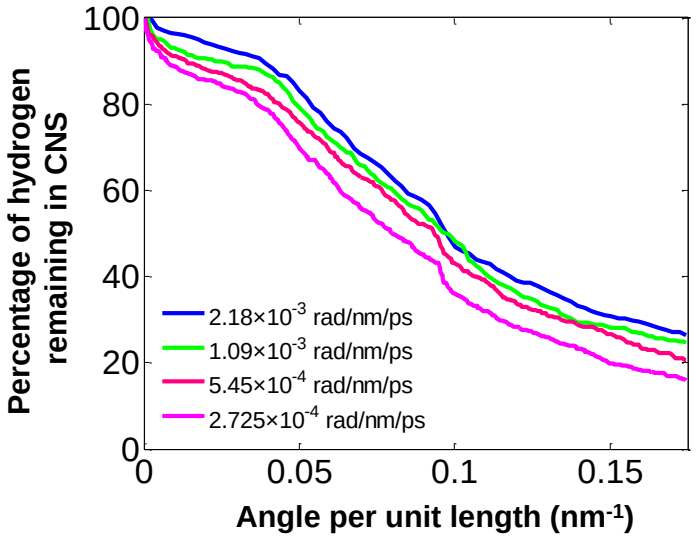

Figure 2.5 Percentage of hydrogen molecules remaining inside the CNS as a function of twisting angle per unit length, for four different loading rates.

2.3.2. Discussion

At a low loading rate, the development of the buckling deformation of the CNS becomes more gradual, which in turn allows the transportation of the hydrogen molecules to be smoother, and thereby the vdW interactions between carbon and hydrogen can play a more effective role in facilitating the mass transportation. Nonetheless, the molecular mass transportation mechanism enabled by torsional buckling instability is shown to be robust over a range of loading rate.

2.4. Molecular Hydrogen Transportation Enabled by Surface Energy Induced Radial Shrinking of a CNS

2.4.1. Energetics of CNS

Next we demonstrate another mechanism to achieve molecular mass transportation via CNSs. Unlike the closed tubular structure of a CNT, the open spiral structure of a CNS indicates that the CNS core size may be tuned by external stimuli [36, 49]. For instance, Gao et al. showed that CNSs respond to an applied DC or AC field by shrinking or expanding their core size [36].

Energetically, the equilibrium shape of a CNS (and thus its core size) is governed by the competition between the surface energy (van der Walls energy) and scrolling-associated strain energy of the basal graphene. Figure2.6 plots the total energy variation during the scrolling process. Before the two edges of graphene overlap with each other, the curling up of basal graphene leads to an increase of strain energy (configuration 1-8 in Figure 2.6) but the surface energy remains 0. Therefore the total energy keeps increasing during this process. Once the two edges meet each other as the bending accumulates, the surface energy decreases and drives the further spontaneous scrolling of the graphene because the total energy decreases (configuration 8-10 in Figure 2.6). The resulting CNS has a lower energy than the original planar graphene. Therefore, the CNS can be stabilized.

It has been shown that the core radius of a CNS is dependent on the surface energy, the C-C interlayer spacing, the bending stiffness and the length of its basal graphene [38] which are correlated by equation,

$$\frac{2\gamma t}{D} = \frac{1}{r_0} - \frac{1}{\sqrt{\left(\frac{Bt}{\pi}\right) + {r_0}^2}}$$

where B is the basal graphene length, r_0 is the inner core radius, t is the interlayer spacing, D is the bending stiffness, and γ is the surface energy per unit area. Particularly, an increased surface energy of the basal graphene can balance more scrolling-associated strain energy of the basal graphene, and therefore result in a tighter CNS with a smaller core radius at equilibrium. In other words, the inner core size of a CNS can be varied if the surface energy of its basal graphene can be tunable. Therefore, manipulation of such a surface energy will potentially provide a way to control the morphology of a CNS. For example, it has been shown that an applied electric field can lead to the polarization of the carbon atoms in a CNS, which in turn results in dipole-dipole interaction energy [36]. Therefore, the effective surface energy of the CNS consists of the contribution of both the C-C vdW interaction energy and the dipole-dipole interaction energy, i.e., $\gamma_{eff} = \gamma_{vdW} + \gamma_{dipole}$. As a result, the effective surface energy of the CNS can be varied by changing the applied electric field, and consequently the core size of the CNS can be tuned over a broad range. Such a tunable core size of the CNS has been shown to facilitate tunable water transport [36].

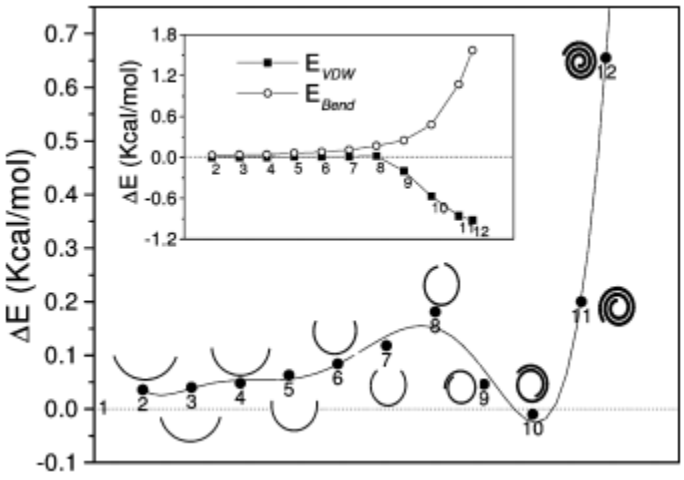

Figure 2.6 Change in total energy during scrolling of graphene to make a CNS. The strain energy and the van der Waals energies are shown in the inset graph [36]

2.4.2. Simulation model and results

In this section, we use MD simulations to demonstrate molecular hydrogen transportation enabled by radial shrinking of a CNS due to the change of surface energy of the basal graphene.

To simulate the collective effect of surface energy on the CNS morphology, a tuning factor λ is introduced in the non-bonded Lennard-Jones potential to represent the change in effective surface energy. The carbon-carbon interaction is thereby described by a Lennard-Jones pair potential $V_{CC}(r) = 4\lambda\varepsilon_{CC}(\frac{\sigma_{CC}^{12}}{r^{12}} - \frac{\sigma_{CC}^{6}}{r^{6}})$, where r is the C-C atomic pair distance, $\varepsilon_{CC} = 2.844 \times 10^{-3} eV$ and $\sigma_{CC} = 3.4\, nm$. To capture the associated change in the hydrogen-carbon non-bonded interaction, the Lorentz-Berthelot mixing rules [52] are applied so that the hydrogen-carbon interaction is

given by a Lennard-Jones pair potential $V_{CH}(r) = 4\sqrt{\lambda}\varepsilon_{CH}(\frac{\sigma_{CH}^{12}}{r^{12}} - \frac{\sigma_{CH}^{6}}{r^{6}})$, where r is the hydrogen-carbon atomic pair distance, $\varepsilon_{CH} = 2.998 \times 10^{-3} eV$ and $\sigma_{CH} = 3.18\, nm$.

A CNS with hydrogen molecules adsorbed inside its core as described in Section 2 is used as the starting configuration in the simulation. The simulation is carried out with Canonical Ensemble at a temperature of 70K and a time step of 0.001 ps. We first set λ to be 7. The increased surface energy of the basal graphene leads to a tighter CNS structure; therefore the core shrinking of the CNS drives the transportation process of hydrogen adsorbed inside the CNS. Such a process is illustrated in Figure 2.6.

When an increase surface energy of the basal graphene is exposed at the beginning of the simulation, the CNS shrinks as the original equilibrium interlayer spacing no longer corresponds to the minimum energy state. As shown in Figure 2.6, at t = 5 ps, the CNS has already tightened a little bit with a few hydrogen molecules squeezed out from the ends of the CNS. The CNS continues tightening with its core size shrinking until t = 20 ps, at which about 65% of the adsorbed hydrogen molecules are pushed out of the CNS. The hydrogen transportation process here is essentially driven by the shrinking core size of the CNS, which is in turn governed by the surface energy of the basal graphene. To reveal the quantitative dependence of the efficiency of molecular mass transportation on the change of surface energy, we conduct further simulations with a set of tuning factors of surface energy (λ = 3, 5, 6, and 7) and compare the results in Figure 2.6.

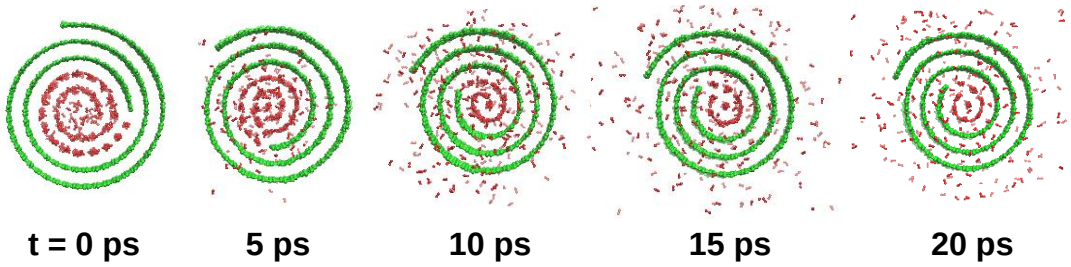

Figure 2.7 Sequential snapshots of the hydrogen molecules (red) initially adsorbed inside a CNS (green) being squeezed out of the CNS due to the radial shrinkage of the CNS driven by a sudden increase of the surface energy of the basal graphene. For visual clarity, the hydrogen molecules initially outside of the CNS are not shown.

It shows that the larger the change in the surface energy of the basal graphene, the faster the CNS core shrinking process attains its equilibrium as indicated by the relatively earlier transition to the plateau regime of the curves in Figure 2.8. Also emerging from Figure 2.8 is that as the change in the effective surface energy increases, the efficiency of the hydrogen molecule transportation improves, which can be understood by the smaller resultant core size of the CNS for a higher surface energy of the basal graphene. For example, as shown in the simulation results, the resultant core diameters of the CNS for λ = 3, 5, 6, 7 are 1.95 nm 1.53 nm, 1.42 nm, 1.26 nm, respectively (Figure 2.8b). The simulation results in this section show that, radial shrinkage of a CNS by tuning the surface energy of its basal graphene could be another potential effective mechanism of molecular mass transportation via CNSs.

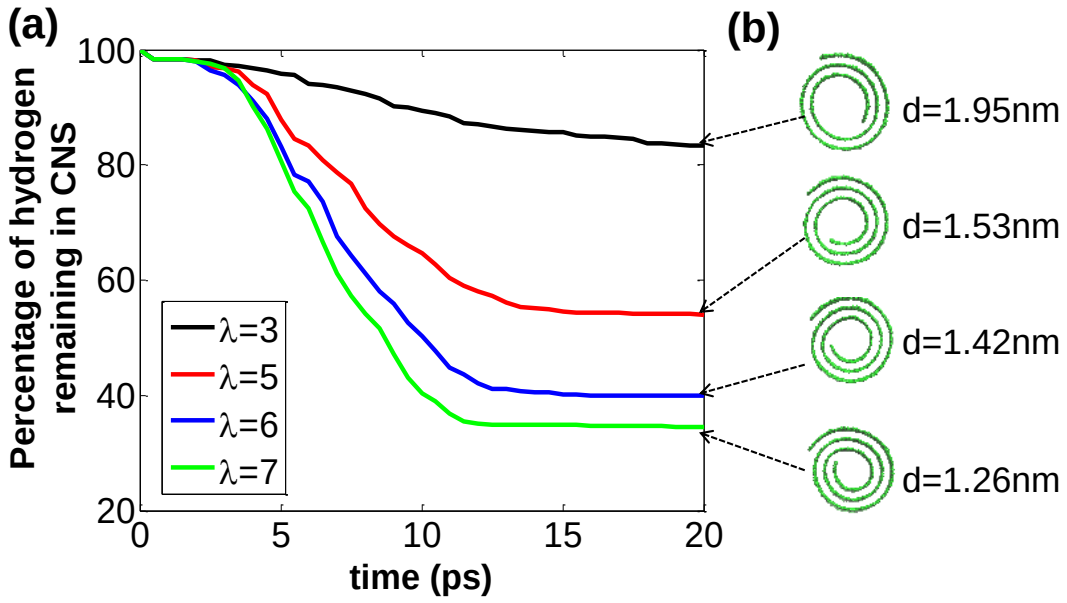

Figure 2.8(a) Percentage of hydrogen molecules remaining inside the CNS as a function of simulation time, for four different tuning factors of surface energy of the basal graphene. (b) End view and resultant inner core diameter of the CNS at the end of the simulation for each case. For visual clarity, hydrogen molecules are not shown.

2.5. Summary

In this Chapter, using MD simulations, we demonstrate two effective hydrogen molecule transportation mechanisms via CNSs enabled by the torsional buckling instability of the CNS and surface energy induced radial shrinkage of the CNS. It is shown that a high efficacy of hydrogen molecule transportation up to about 80% can be achieved by leveraging the torsional buckling instability of the CNS and such a transportation mechanism is robust over a range of torsional loading rates. If a sufficiently large change in the surface energy of the basal graphene can be achieved, the resulting radial shrinkage can also lead to hydrogen molecule transportation with

a reasonable efficacy. As the two transportation mechanisms demonstrated in this paper are essentially driven by the non-bonded interaction of the hydrogen molecules and the basal graphene of the CNS, it is expected that the similar mechanisms are applicable for the transportation of molecular mass of other types, such as water molecules, DNAs, fullerenes and nanoparticles. While the simulation results presented here are promising, there are challenges that are crucial for the experimental realization of the demonstrated molecular mass transportation mechanisms. For example, it remains largely unexplored how to manipulate a CNS with sufficient precision to apply mechanical loads and how to significantly tailor the surface energy of a CNS without severely compromising the structural integrity of the basal graphene. We therefore call for further experimental explorations of the molecular mass transportation mechanisms envisioned by the present study.

Chapter 3: Directional Transport of Molecular Mass on Graphene by Straining

Directional transport of molecular mass is essential in enabling desirable functions in nano-devices, but is often challenging to achieve. In this Chapter, we combine theoretical analysis and molecular simulations to demonstrate a facile mechanism of directional transport of molecular mass on graphene by a simple stretch. In Section 3.2, we reveal that stretch-induced strain gradient in graphene leads to a net transport force that is sufficient to drive molecular cargo on the graphene in a directional and programmable fashion. In Section 3.3, simulation results are provided to demonstrate the feasibility of this approach. Potential applications are envisioned in Section 3.4. As summarized in Section 3.5, the large elastic deformability of graphene and the van der Waals nature of the transport force allow for programmable directional transport of various types of molecular cargo (e.g., graphene flake, carbon nanotube, fullerene, and gold nanoparticle) under the same mechanism. The present findings suggest a fundamental law of directional transport of molecular mass by straining.

3.1. Background

Directional transport of molecular mass is of great importance in designing novel molecular devices and machines, and has a wide range of potential applications in fields such as micro/nano fluids, nanorobotics and nanoelectromechanical systems [53-58]. External mechanical, electrical or magnetic excitations have been shown to

induce directional motion of molecular mass [54, 59-62]. For example, an excited vibrating carbon nanotube cantilever can act as an efficient nanopump [59]. The presence of a gradient in a potential field can also cause directional motion of molecular mass, mimicking the fact that in macroscopic regime objects tend to fall towards lower gravity potential direction. For example, thermal gradient has been experimentally and theoretically studied on its role of enabling fullerene, graphene flakes, and other molecular cargos to migrate towards lower temperature region on a graphene surface [55, 63-65]. Surface chemical gradient, surface tension gradient, surface structural-scale gradient have been demonstrated to be effective to transport water droplet [66-69]. It has been theoretically shown that controlled variations of the intensity or phase of a DC/AC electric field can pump water molecules through carbon nanotubes [70, 71]. The above transport mechanisms of molecular mass, however, suffer from either complicated multi-physics actuation scheme, or lack of active control of the transport direction. A facile mechanism of directional transport of molecular mass is still highly desirable.

Introducing strain in graphene by wrinkling [72-74], folding [75-27] and functionalization [78-83] in a programmable fashion have received enormous attention, largely due to the need to actively control the electronic and structural properties of graphene [84-90]. Nevertheless few efforts have been made to explore the effect of straining graphene on directional transport of molecular mass. In this Letter, through theoretical modeling and molecular simulations, we show that a strain gradient in graphene can generate a net transport force on a molecular cargo on the graphene that is sufficient to drive the motion of the molecular cargo in a controlled

direction. Given the high elastic deformability of graphene and the facile reversibility of applied straining, programmable transport of molecular mass on graphene can be achieved. The net transport force is essentially van der Waals (vdW) type, therefore such a transport mechanism can be applicable to transport a wide range of molecular cargos on various platforms. Results from the present study can potentially offer a fundamental law of directional transport of molecular mass by straining.

3.2. Theoretical Framework of Net Transport Force on Molecular Mass Induced by a Strain Gradient in Graphene

3.2.1. A single atom model

For an atom positioned above a pristine graphene, the total interaction force between the atom and the graphene can be determined by summing up all atomic-pair potentials between the atom and all carbon atoms in the graphene. Such a potential for an atomic pair of distance r due to vdW force is usually represented by a Lennard-Jones 6-12 potential, $V(r) = 4\epsilon\left(\frac{\sigma^{12}}{r^{12}} - \frac{\sigma^{6}}{r^{6}}\right)$, where $\sqrt[6]{2}\sigma$ is the equilibrium distance between atoms and ϵ is the bond energy at the equilibrium distance. Due to the symmetry of graphene lattice, such a total interaction force zeros out when the atom is positioned with a separation distance from graphene of $h = \sqrt[6]{2}\sigma$. As a result, the atom reaches equilibrium and does not move in a preferred direction. By contrast, when the basal graphene is subject to a strain gradient, the graphene lattice symmetry

is broken; there exists a net force acting on the atom, essentially due to the uneven distribution of the carbon atoms in the graphene, as to be detailed below.

Consider a rectangular basal graphene of length L, subject to uniaxial in-plane tension perpendicular to its length direction (Figure 3.1.a). The applied tension linearly decreases from e_{max} at one end to zero at the other end of the graphene. In other words, the graphene is subject to a strain gradient of e_{max}/L. An atom is positioned above the graphene with a separation distance of h. In order to establish a semi-continuum cohesive law between the atom and the graphene, we homogenize carbon atoms in the graphene and represent them by an area density ρ_s. The cohesive energy Φ between the atom and the graphene is therefore given by [73, 91]:

$$\Phi = \int V(r)\rho_s dxdy = 4\epsilon\rho_s\pi\left(\frac{\sigma^{12}}{5h^{10}} - \frac{\sigma^{6}}{2h^{4}}\right). \quad (1)$$

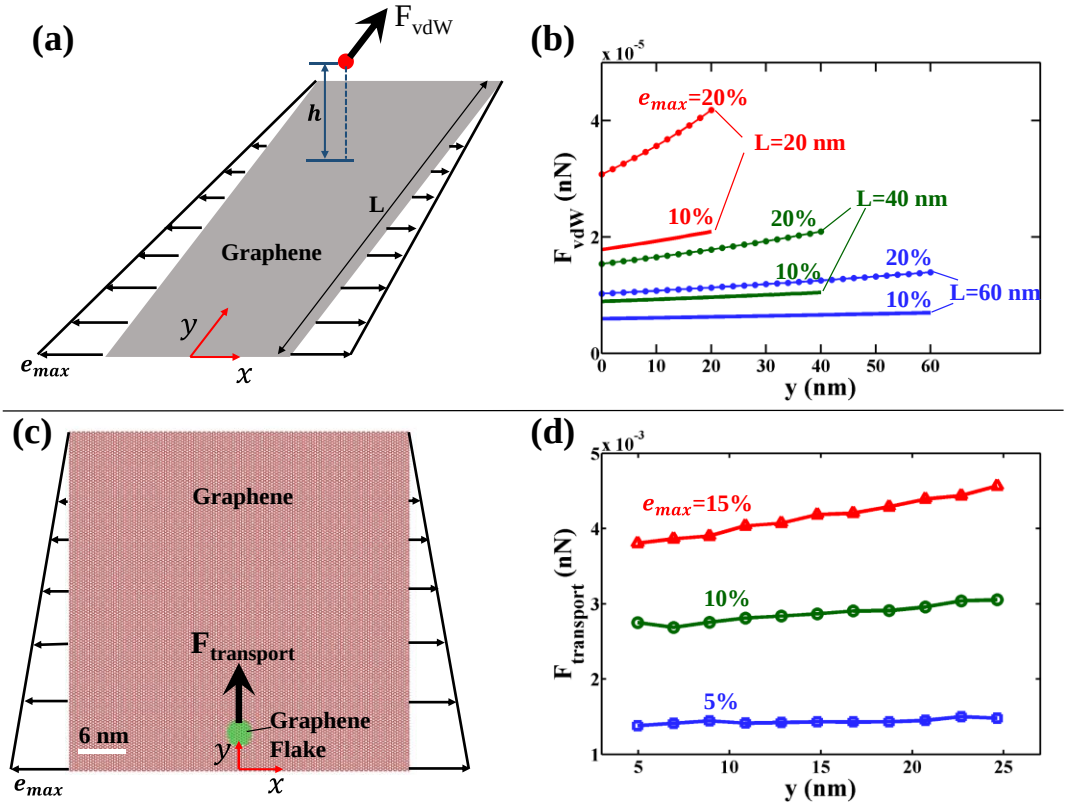

Figure 3.1(a) Schematic showing that a net force F_{vdW} acting on an atom (red dot) positioned above on a basal graphene subject to a strain gradient points to the decreasing strain direction. (b) F_{vdW} as a function of position along *y* direction for various lengths of basal graphene and strain gradients. (c) Molecular mechanics model of a round graphene flake on a basal graphene subject to a strain gradient to compute the overall net force $F_{transport}$ acting on the graphene flake, which is plotted as a function of position along *y* direction for various strain gradients (d).

The relation between the area density ρ_s of deformed graphene under strain (e_x, e_y) and the area density ρ_0 of pristine graphene is given by

$$\rho_s = \frac{\rho_0}{1+e_x+e_y+e_x e_y} \cong \frac{\rho_0}{1+e_x+e_y} \tag{2}$$

Given the uniaxial tension, $e_y = -\nu e_x$, where ν is the Poisson's ratio. This leads to

$$\Phi = \frac{4\epsilon\rho_0\pi}{1+(1-\nu)e_x}\left(\frac{\sigma^{12}}{5h^{10}} - \frac{\sigma^6}{2h^4}\right) \tag{3}$$

A net force acting on the atom from the deformed graphene is then given by

$$F_{vdW} = -\frac{d\Phi}{dy} = \frac{4\epsilon\rho_0\pi}{(1+(1-\nu)e_x)^2}\left(\frac{\sigma^{12}}{5h^{10}} - \frac{\sigma^6}{2h^4}\right)(1-\nu)\frac{de_x}{dy} \tag{4}$$

Assume a linear distribution of uniaxial tension in the graphene, so that

$$e_x = (1-\frac{y}{L})e_{max} \tag{5}$$

At the equilibrium separation distance, $h = \sqrt[6]{2}\sigma$. Therefore,

$$F_{vdW} = \frac{\frac{4}{5}\epsilon\rho_0\pi h^2}{\left(1+(1-\nu)(1-\frac{y}{L})e_{max}\right)^2}(1-\nu)\frac{e_{max}}{L} \tag{6}$$

Figure 3.1.b plots F_{vdW} as a function of the location of the atom along *y* direction, for various lengths of basal graphene (20 nm, 40 nm, and 60 nm,

respectively) and e_{max} (10% and 20%, respectively). Here $\epsilon = 0.00284\ eV, h = 0.34\ nm, \rho_0 = \frac{4}{3\sqrt{3}l_0^2}, l_0 = 0.142\ nm$, which are representative for the carbon-carbon vdW interaction. Figure 3.1.b shows that there exists a net force F_{vdW} acting on a carbon atom above a basal graphene subject to a strain gradient, pointing to the decreasing strain direction. In general, a higher strain gradient in the basal graphene (e.g., larger e_{max} for a fixed L, or shorter L for a fixed e_{max}) leads to a larger net force. Similarly, for a given e_{max}, a shorter basal graphene (thus a higher strain gradient) causes a larger net force. F_{vdW} also increases slightly as the location of the atom moves toward the decreasing strain direction. Given that the nature of vdW type interaction, it is expected that such a net force also exists for an atom of different type above a basal graphene subject to a strain gradient.

3.2.2. Validation by simulation

When a molecular cargo is positioned on a basal graphene under a strain gradient, an overall transport force $F_{transport}$, acting on the cargo and pointing toward the decreasing strain direction, exists and can be computed by summing up all net force acting F_{vdW} on individual atoms in the molecular cargo. To verify the above theoretical consideration, we next perform molecular mechanics simulations to compute $F_{transport}$ acting on a round graphene flake with a diameter of 2.3 nm above a basal graphene of 30 nm by 30 nm subject to a strain gradient, as shown in Figure 3.1c. With the center of mass of the round graphene flake being hold in the equilibrium position to the basal graphene, energy minimization is performed using large-scale atomic/molecular massively parallel simulator (LAMMPS) [50], in which

the carbon material structure is described by the adaptive intermolecular reactive empirical bond order (AIREBO) potential [46]. $F_{transport}$ acting on the graphene flake is computed by summing all carbon-carbon atomic pair potentials between the graphene flake and basal graphene. Figure 3.1.d plots $F_{transport}$ as a function of flake position along *y* direction for various strain gradients in the basal graphene. A higher strain gradient in the basal graphene leads to a larger overall transport force $F_{transport}$ acting on the graphene flake. $F_{transport}$ also slightly increases as the graphene flake is positioned further along the decreasing strain direction. The molecular mechanics simulation results in Figure 3.1.d are in line with the prediction from the theoretical mechanics model in Figure 3.1.a, validating the underlying mechanism of directional transport of molecular mass on graphene via straining. As to be further shown by the molecular dynamics (MD) simulations in the next section, the overall transport force $F_{transport}$ acting on a molecular cargo is sufficient to drive the cargo to move in a controllable fashion on the basal graphene at room temperature.

3.3. Directional Transport of Molecular Mass on Graphene by Straining

In this section, we use MD simulations to demonstrate directional transport of various types of molecular mass on a basal graphene by programming the applied strain gradient. All MD simulations are performed using LAMMPS, with the

temperature kept at 300 K using canonical ensemble. All carbon material structure is described by the AIREBO potential.

Figure 3.2 demonstrates directional transport of a round graphene flake of 2.3 nm in diameter on a graphene nanoribbon (GNR) of 30 nm by 4 nm. Under a strain gradient with $e_{max} = 15\%$, the net transport force acting on the round graphene flake drives it to start moving toward the decreasing strain direction on the GNR, and reaches the center of the ribbon at 168 ps and the end of the ribbon at 236 ps. The accelerating fashion of the transport process agrees with the steady driving force predicted in Figure 3.1.d. Due to the trapping effect of the graphene edge [92], the round graphene flake bounces back once hitting the zero-strain end of the GNR. The net driving force due to strain gradient further causes the graphene flake to approach the zero-strain end again, arriving with a lower velocity. Eventually the round graphene flake stabilizes around the zero-strain end of the GNR. Upon reversing the direction of strain gradient (with the same amplitude) in the GNR, the net transport force acting on the graphene flake can overcome the trapping effect of the now higher-strain end of the GNR, so that the graphene flake starts to move in the opposite direction. Once the graphene flake is away from the end of the GNR, the steady net transport force drives it to move in an accelerating fashion. The graphene flake eventually stabilizes at the zero-strain end of the GNR under the interplay of net transport force and edge trapping effect of graphene. The above simulation case demonstrates that programmable directional transport of molecular mass can be achieved by devising the strain gradient profile in the basal graphene.

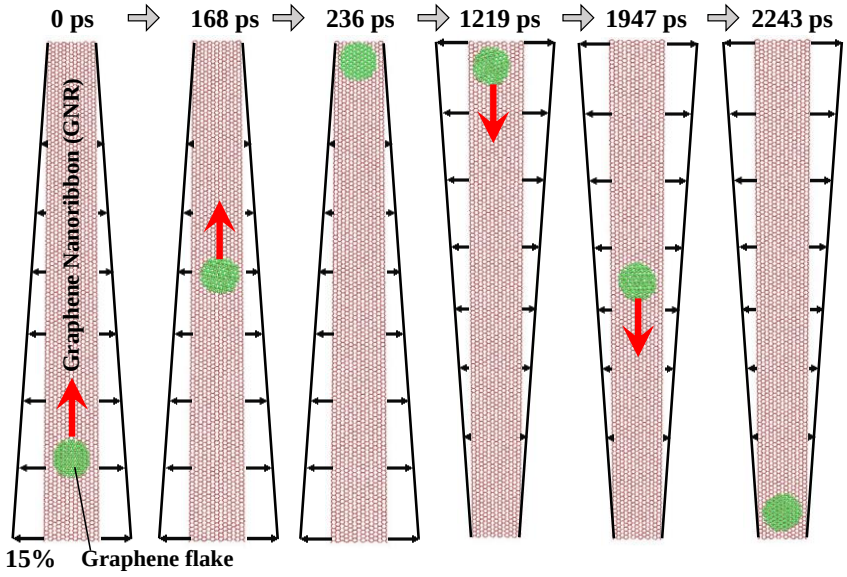

Figure 3.2 Snapshots of MD simulations of programmable directional transport of a round graphene flake (green) on a graphene nanoribbon (GNR) by controlling the strain gradient in the GNR.

Figure 3.3 demonstrates directional transport of a carbon nanotube (CNT) on a GNR subject to a strain gradient. A (36, 0) CNT with 2.8 nm in length is positioned at one end of a GNR of 3 nm by 30 nm (Figure 3.3.a). The net transport force on the CNT due to a strain gradient in the GNR with $e_{max} = 15\%$ causes the CNT to migrate on the GNR toward the decreasing strain direction (Figure 3.3b). By highlighting several rows of carbon atoms in the CNT, it is found that the transport process is achieved by a mixing of sliding and rolling of the CNT on the GNR (see Supplementary Materials for a simulation video). While the sliding of the CNT on the GNR results from the net transport force pointing to the decreasing strain direction, the rolling of the CNT can be understood as following: The vdW interaction between the CNT and the GNR causes the deformation of the CNT cross-section into a shape

with a flat portion in direct contact with the GNR (with an interlayer distance close to that of a graphene bilayer) and the rest curving portion due to the bending rigidity of the CNT cross-section. Away from the equilibrium interlayer distance, the curving portion of the CNT is subject to a vdW attraction from the GNR in the vertical direction. Due to strain-gradient-induced difference in area density of carbon atoms in the GNR (e.g., Eq. 2), the overall vdW attraction in the vertical direction acting on the half of the CNT at the lower strain side is greater than that at the higher strain side, as illustrated in Figure 3.3.c, leading to a net torque that drives the CNT to roll on the GNR toward the decreasing strain direction.

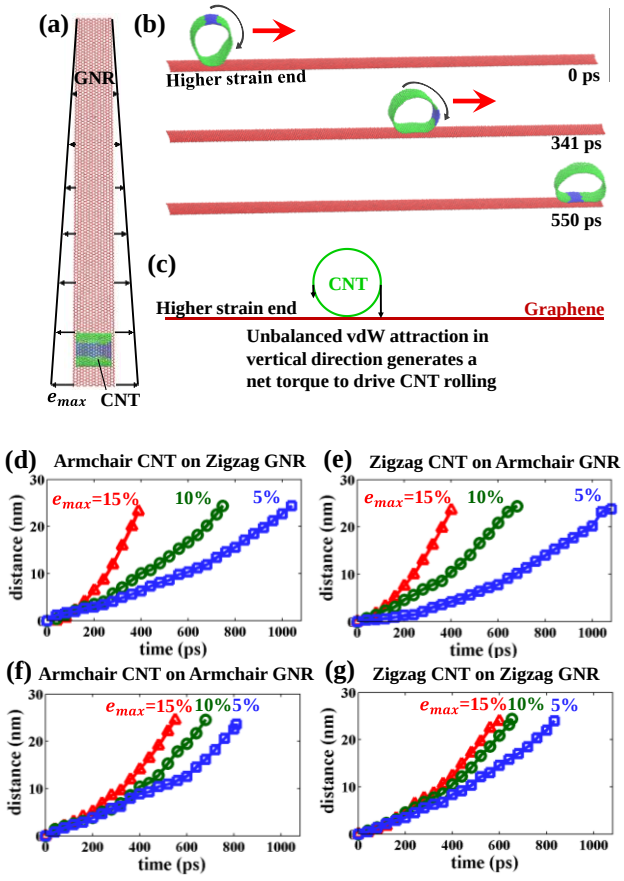

Figure 3.3 MD simulations on directional transport of a CNT on a GNR subject to a strain gradient. (a) Schematic of simulation model and applied strain gradient. (b) Snapshots of the transport process of the CNT toward decreasing strain direction. Several rows of carbon atoms in the CNT are shaded in blue to reveal the CNT rolling on the GNR (see Supplementary Materials for a simulation video), resulting from a net torque due to unbalanced vdW attraction in vertical direction acting on the CNT (c). (d-g) Transport distance of the CNT as a function of simulation time for various e_{max} and combinations of chirality of the CNT (by its edges) and the GNR (by its longer edges).

Further simulations (Figure 3.3.d-3.3.g) show that the strain-gradient-driven transport of a CNT on a GNR can be effectively achieved for various combinations of CNT and GNR chirality. Given the limiting cases in terms of chirality combinations in Figure 3.3.d-3.3.g, the strain-gradient-driven transport mechanism of CNT on GNR is expected to be robust. Also as shown in Figure 3.3d-3.3.g, the higher the strain gradient in the GNR (i.e., higher e_{max} for a fixed GNR length), the faster the transport process, which can be readily explained by the higher transport force as predicted in Section 2 (e.g., Figure 3.1.d).

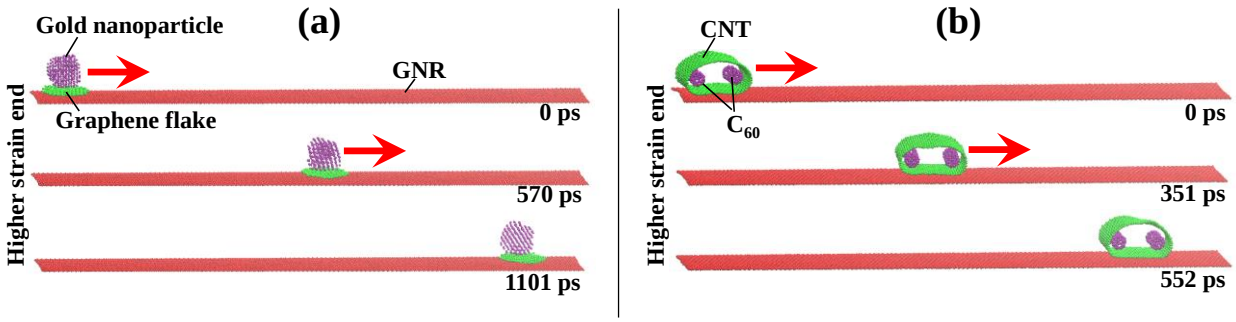

Figure 3.4 MD simulations of the directional motion of various molecular cargos on a GNR subject to a strain gradient. (a) A gold nanoparticle (purple) on a round graphene flake (green). (b) Four C_{60} molecules (purple) housed in a CNT (green).

Figure 3.4 further demonstrates that a graphene flake or a CNT can be used as a vehicle to shuttle other molecular cargos on a GNR under the same mechanism. As shown in Figure 3.4.a, a gold nanoparticle with a radius of 1 nm is placed on a round graphene flake with a radius of 1.3 nm sitting on a GNR subject to a strain gradient with $e_{max} = 10\%$. In the simulations, the gold atoms are described by the embedded atom method (EAM) potential [93], and the vdW interaction between a gold atom and a carbon atom is modeled by a Lennard-Jones 6-12 potential, in which $\epsilon_{Au-C} = 0.0127\ eV, \sigma_{Au-C} = 0.2994\ nm$ [94], indicating a much stronger interaction between the gold nanoparticle and the round graphene flake than that between the flake and the GNR. The transport force due to strain gradient in the GNR drives the graphene flake to move toward the decreasing strain direction. With the graphene flake moving away from its equilibrium location with the gold nanoparticle, the vdW interaction between them becomes attractive. As a result, the gold nanoparticle is pulled by the graphene flake to start to move toward the decreasing strain direction, meanwhile the graphene flake is dragged by the gold nanoparticle to first slow down until stop and then start to move toward the opposite direction. Once the graphene flake moves behind the gold nanoparticle, the vdW interaction between them first slows down the graphene flake to stop and then further drives the flake to move toward the decreasing strain direction again. The above interplay between the graphene flake and the GNR and that between the flake and the gold nanoparticle, on one hand, lead to the overall

motion of the cargo (gold)-loaded vehicle (graphene flake) toward the decreasing strain direction; and on the other hand, due to the much larger mass (thus the inertia) of the gold nanoparticle than that of the graphene flake (7.85×10^{-20} g vs. 0.40×10^{-20} g), the graphene flake also oscillates locally back and forth with respect to the gold nanoparticle (see Supplementary Materials for a simulation video). Figure 4b further shows that a CNT can serve a vehicle to carry four fullerene (C_{60}) molecules and shuttle them along a GNR subject to a strain gradient with $e_{max} = 10\%$, in a similar fashion as shown in Figure 3.3. With cargo (C_{60}) loaded, the CNT has a larger flat portion than that in Figure 3.3, leading to a transport process with more sliding than rolling of the CNT. Nonetheless, simulations in Figure 3.4 clearly demonstrate that the strain-gradient-driven transport mechanism can be generally applicable to achieve directional transport of various types of molecular mass in a programmable fashion.

3.4. Potential Application

The underlying mechanism of the strain gradient induced net transport force is due to the unbalanced atom density in graphene caused by non-uniform strain field. A higher local strain in graphene leads to a lower local atom density, and vice versa. Since the vdW force is directly proportional to the atom density (e.g., Eq. 1), therefore when a basal graphene is subject to a strain gradient, a non-zero net vdW force acts on a molecular cargo above the graphene in the direction pointing to the decreasing strain direction. Such a mechanism can be feasibly extended to design other potential directional transport schemes.

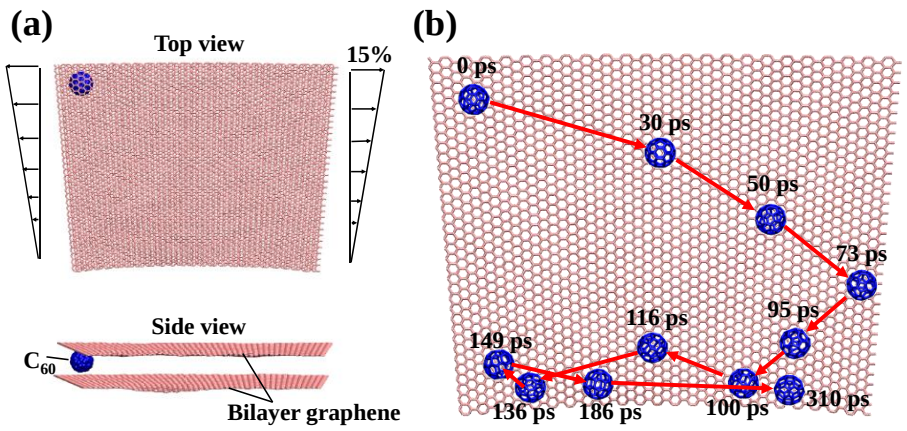

Figure 3.5 MD simulations on the pumping effect in a graphene bilayer nanochannel induced by a strain gradient. (a) Top view and side view of a C_{60} molecule located near the top end of a graphene bilayer nanochannel subject to a strain gradient. The maximum applied strain is 15%. (b) The trajectory of the C_{60} molecule in the graphene bilayer nanochannel. For visual clarity, the top graphene layer is not shown.

For example, graphene bilayers have been proposed to serve as nanofludic channels to conduct nanoliquid under infiltration pressure [95-98]. As a demonstration, here we show that a strain engineered graphene bilayer nanochannel can enable directional transport of molecules without the need for infiltration pressure. Figure 7(a) shows the top and side views of the graphene bilayer nanochannel with a C_{60} molecule located at the top end. When the graphene bilayer nanochannel is subject to a strain gradient, a net transport force acts on the C_{60} molecule and drives it to move downward. Figure 7(b) shows the trajectory of the C_{60} molecule. At 73 ps, the C_{60} molecule hits the boundary of the nanochannel, bounces back due to the graphene edge effect [92] but still moves downwards. At 100 ps, the C_{60} molecule reaches the bottom end of the nanochannel, bounces back a shorter

distance and then moves downwards again. After several cycles of bouncing upwards and accelerating downwards, the C_{60} molecule eventually stabilizes at the bottom end of the nanochannel. Such a bouncing feature until stabilizing at the bottom is analogous to that of a ball after being dropped onto the ground. This example clearly offers further evidence that a considerable net vdW force (analogous to gravity) acts on the molecular cargo towards the decreasing strain end, indicating a promising solution for pumping nanofluids via graphene nanochannels in a programmable fashion.

3.5. Summary and Discussions

In this Chapter, we demonstrate a facile and robust mechanism of directional transport of molecular mass by straining. Theoretical analysis and molecular simulations show that a strain gradient in a graphene can generate a net transport force to actuate and drive a molecular cargo on the graphene to move toward the decreasing strain direction. The vdW nature of the transport force and the programmable feature of the straining scheme promise such a mechanism to be robustly applicable to a broader range of material systems (for both molecular cargo and transport platform), as exemplified by the various demonstrations presented in this Letter. We therefore call for further systematic explorations of the fertile opportunities offered by this fundamental law of directional transport of molecular mass by straining.

Chapter 4: Line Defects Guided Molecular Patterning on Graphene

Graphene emerges as a candidate scaffold for patterning molecules. However, with existing techniques it still remains unclear how to achieve molecular self-assembly in domains of desirable geometry. In this Chapter, we reveal a barrier effect of line defects (e.g., open slits) in graphene (Section 4.2), which can potentially enable molecular confining and patterning in a domain of desirable geometry. Using molecular dynamics simulations, we demonstrate that fullerene molecules can be readily patterned into a stable cluster of various shapes and sizes (Section 4.3). Such a strategy is expected to be applicable to pattern various types of molecules that interact with graphene via van der Waals. The simulation models and results are summarized in Section 4.4.

4.1. Background

Molecular self-assembly has received great attention in nanotechnology in recent years, driven by its promising potential to pattern random molecules into structures with desired property and function [99-102], which in turn, can find possible applications such as molecular storage [103], chemical reaction control[104], and bio-medical systems [102]. Various self-assembly techniques have been studied recently. In particular, the advent of graphene motivates its use as a template for molecular self-assembly due to its unique property. By using molecular dynamics simulations, Shenoy *et al.* have shown that domain of hydrogenated graphene which

is embedded in pristine graphene sheet, the so called “graphone”, can adopt well-defined three-dimensional geometries. These kinds of morphologies can create energy walls to trap molecules inside by means of physisorption [103]. Zettl *et al.* have demonstrated experimentally an artificial layered material synthesis method. This method yields stacks of graphene separated by guest particles of various types. The resulting structure will adopt a “sandwich like” or “veil like” shape, depending on how closely the guest particles are packed with each other, and can be harnessed as two-dimensional platform to control the movements and chemical reaction of guest species [105].

However, the molecular packing geometry in these existing techniques is relatively limited because it still remains unclear how to achieve molecular self-assembly into a pre-defined arbitrary geometry. To address this challenge, in this Chapter we use molecular dynamics simulation to demonstrate a feasible and robust approach to patterning molecules into domains of desired shapes and sizes on graphene by simply introducing line defects (e.g. open slits) in graphene. The underlying mechanism is also illustrated.

Recent progresses in graphene engineering have made it feasible to tailor graphene into desirable shape and also to introduce defects into pristine graphene with atomic resolution, which is the key step in our proposed method. It is reported that cutting graphene with sub-nanometer-precision can be achieved using scanning tunneling microscopy lithography [106] and focused electron beam etching [107]. Researchers have also shown that by using a scanning transmission electron microscope with a 0.1 nm 300 kV electron beam, graphene can be sculpted into

patterns of predefined positions and sizes with close-to-atomic precision. This process can even be automated by using a script, thus become fully computer-controlled to fabricate more complex shapes [108]. Drndic *et al.* shows that features including nanometer-scale pores, point defects and line defects (e.g. open slits and gaps) can be introduced into graphene by knocking off carbon atoms using controlled exposure to focused electron-beam [109] or high-energy ion beam irradiation [110,111], and these features will be stable afterwards and do not evolve over time. These progresses on programmable and controllable introduction of defects in graphene make the proposed molecular patterning method on graphene in this Chapter very feasible to achieve in real experiments.

4.2. Theoretical Foundation

In this Section, we will illustrate the underlying mechanism. At the center of line defect guided molecular patterning on graphene is the "barrier effect" of open slits in graphene, as demonstrated in Figure 4.1. An open slit is introduced in a graphene monolayer by knocking off a row of carbon atoms. The resulting slit has a width of 3 Å and is composed of two zigzag edges. A fullerene (C_{60}) molecule is placed near the slit. Energy minimization is performed using large-scale atomic/molecular massively parallel simulator (LAMMPS), in which the carbon material structure is described by the adaptive intermolecular reactive empirical bond order (AIREBO) potential. The interaction between the graphene and C_{60} is van de Waal (vdW) type. The total vdW force acting on the C_{60} molecule can be computed by summing all carbon-carbon atomic pair potentials between the C_{60} molecule and

the graphene. When the C_{60} molecule is placed on a perfect graphene sheet or far away from the slit, the total in-plane vdW force acting on the C_{60} is nearly zero, given the symmetry of the graphene lattice. By contrast, when the C_{60} molecule is placed near the open slit, the missing carbon atoms at the slit result in a net vdW force acting on the C_{60} molecule in the direction perpendicular to the slit and pointing to the direction away from the slit. In other words, the open slit serves as a barrier by exerting a net force to the C_{60} molecule to push it away. It should be noted that in this molecular mechanics model, the dangling bonds of the edges in defects are not saturated for the simplicity of calculation. However the saturation of edge atoms won't affect the barrier effect because such an effect arises from the uneven distribution of the atoms in basal graphene due to the missing atoms in the defects. As long as there is a line defect, the same result will hold. To increase the strength of the barrier effect, the defect can be made wider to induce a more unbalanced atom density.

To demonstrate such a barrier effect, Figure 4.1 plots the net in-plane vdW force acting on the C_{60} molecule as a function of its distance to the open slit. Initially the C_{60} is placed on the right with a distance d to the center gap of 10 Å and then it is displaced along the horizontal direction towards the open slit with a displacement step of 0.5 Å. The distance from the center of the C_{60} molecule to graphene in out-of-plane direction is fixed at its equilibrium value (~8 Å). At each location, the energy minimization is performed and then the resultant force along the horizontal direction is documented. In this fashion we can obtain the net vdW force in horizontal direction as a function of the distance from the C_{60} to the center of the open slit. As shown in

Figure 4.1, when the C_{60} is far from the slit edge, the net vdW force approaches to zero as the molecule cannot feel the open slit and the vdW force is zero-balanced. As the C_{60} moves toward the slit, the net vdW force increases, which peaks at a distance about 3 Å to the center of the slit in the direction that prevents the C_{60} molecule to move further toward the slit. The net force decreases to zero only when the C_{60} is placed right above the center of the open slit due to symmetry. Essentially, such a net force results from the difference between the carbon atom density of graphene on the right side and that on the left side of the C_{60} molecule as it approaches the open slit. The higher atom density side (i.e., away from the open slit) provides a vdW force greater than the less dense side. As a result, the effectively pulls the C_{60} molecule away from the edge of the open slit. Figure 4.1 also plots the net force vs. distance from the edge of an open slit along the armchair direction, which shows a rather similar trend. Due to the symmetry of the graphene lattice, the two curves in Figure 4.1 set the upper and lower limits of the net force due to an open slit along arbitrary direction in graphene. The barrier effect of an open slit in graphene demonstrated in Figure 4.1 is the physical origin of the proposed approach to packing molecules in a domain of desirable shape as shown in the following.

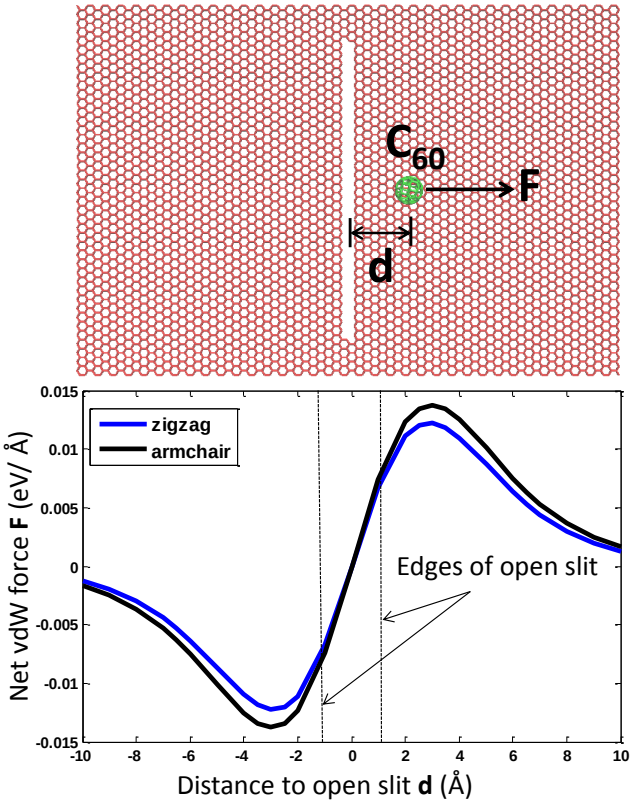

Figure 4.1 (a) A 3 Å-wide open slit is introduced in a graphene monolayer by knocking off a row of carbon atoms and is composed of two zigzag edges. A C_{60} molecule is placed near the slit with an out-of-plane distance of 8 Å to the graphene sheet. (b) Net in-plane vdW force acting on the C_{60} as a function of the distance of C_{60} to the open slit. Dashed lines mark the location of the edges of the open slit.

4.3. Simulation Results

4.3.1. C_{60} molecules patterned in square shaped domain

As an example of the above mentioned barrier effect of open slits, we demonstrate molecules packing in a square-shaped domain. As shown in Figure 4.2, four slits with length of 50 Å and width of 3 Å are introduced in a square-shaped

graphene sheet (100 Å by 100 Å), demarcating a smaller square-shaped domain. Then nine C_{60} molecules are randomly introduced to the central square-shaped domain (Figure 4.2a, e.g., by dispersing C_{60} molecules over the graphene), and the system then evolves freely at 300K. Driven by thermal fluctuation, the C_{60} molecules start to move around. When a C_{60} moves toward the open slits, it will be bounced back into the square-shaped domain due to the barrier effect (see Supplemental Materials for a simulation video). Figure 4.2a-4.2c shows the snapshots of the confined motion of the C_{60} molecules and the corresponding patterning process. In Figure 4.2b, five out of the nine C_{60} molecules cluster together in a triangular pattern, as highlighted by the solid line. Figure 4.2c shows that further self-assembly eventually pattern all C_{60} molecules into a cluster in a triangular lattice, which is driven by reducing vdW energy. Such a cluster moves around as a whole within the domain. The triangular pattern shown in Figure 4.2 is dictated by the vdW interaction among C_{60} molecules and substrate. This ordered pattern is in agreement with simulation and experimental results of previous research [113].

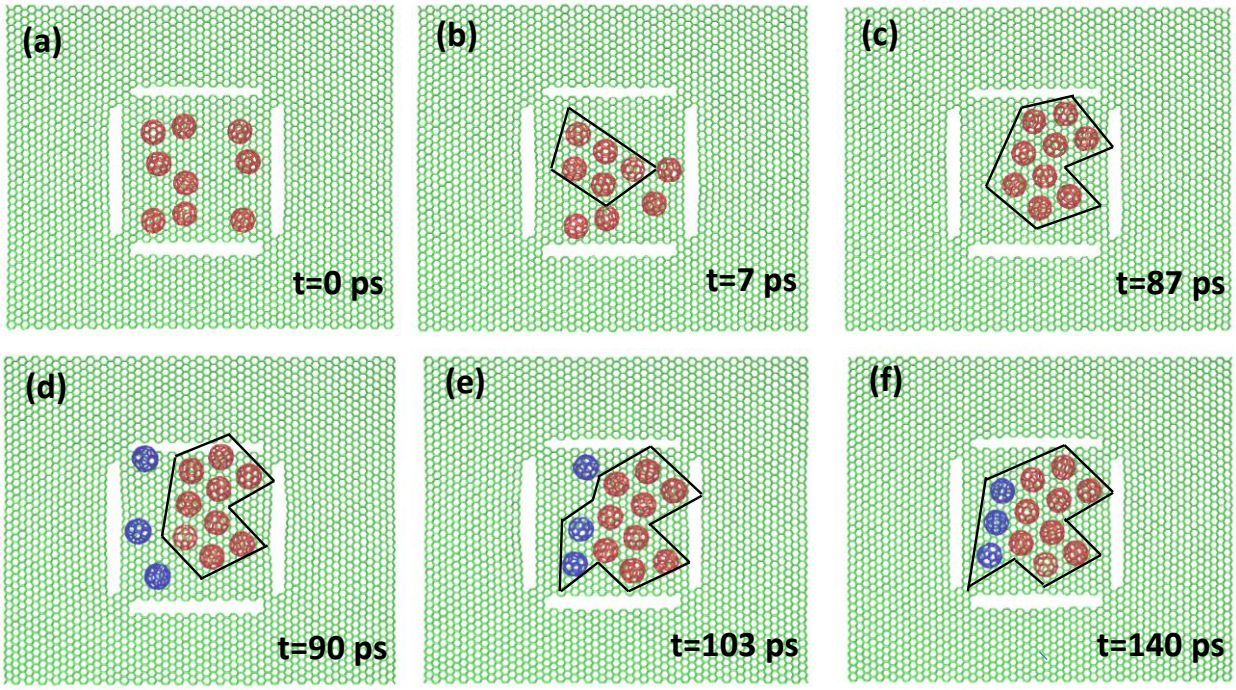

Figure 4.2 (a) Initial configuration of the simulation, nine C60s are randomly distributed in the square-shaped domain enclosed by four slits. (b) At 7 ps, five of nine C60s start to cluster into a triangular pattern. (c) At 87 ps, all nine C60s self-assemble into a larger cluster with a triangular lattice. (d) Three more C60s are added to the existing system. (e) Two of the three newly added C_{60}s are self-assemble into the cluster. (f) All the 12 C_{60}s form a larger cluster with triangular lattice.

Next, we explore the maximum packing capacity by adding more C_{60} molecules into the square-shaped domain. It is shown that further added C_{60} molecules into the square-shaped domain can readily self-assemble into the existing cluster, leading to an even larger cluster (Figure 4.2d-4.2f). The first two snapshots in Figure 4.3 show the evolution of the newly added three C_{60} molecules to the final configuration in Figure 4.2. The similar self-assembly process is observed. As the C_{60} cluster grows in size, its random migration under thermal fluctuation within the

square-shaped domain will become more confined. It is shown that ultimately a total of 23 C_{60} molecules can be densely packed in a 50 Å by 50 Å square-shaped domain (Figure 4.3.h).

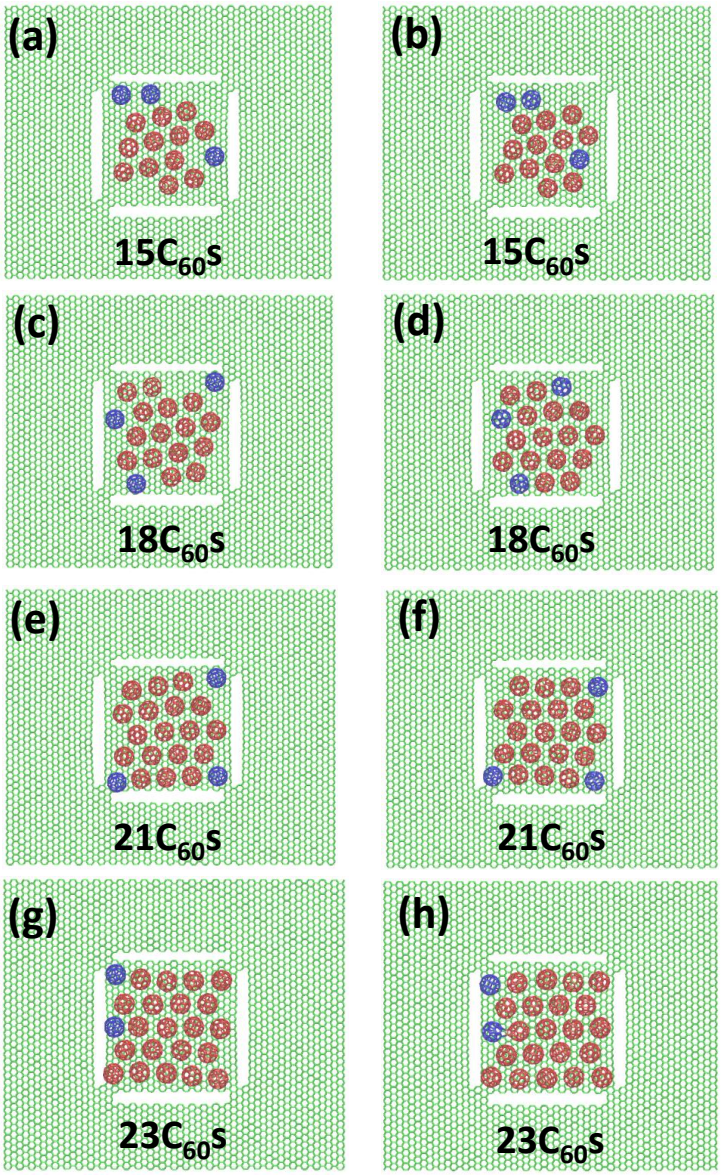

Figure 4.3 More C_{60}s (shown in blue color) are continuously added into the square-shaped domain (left column) step by step, which can readily self-assemble into the existing cluster

(right column) in a well-defined triangular lattice. Eventually the squared domain can accommodate 23 C_{60}s.

4.3.2. C_{60} molecules patterned in domains of arbitrary geometries

As suggested by the results in Figure 4.1, the barrier effect will hold for open slits of any arbitrary direction in a graphene sheet. This renders versatile design of confining domain, which in turn can enable molecules patterning into desirable geometry.

As a demonstration, Figure 4.4 shows patterning C_{60}s into different other shapes, such as triangular, circular and hexagonal. Since the C_{60} cluster self-assembled inside a prescribed confining domain is dictated by the inter-C_{60} vdW interaction and thus energetically favorable (as evident by the thermal motion of the cluster as a whole), it is expected that such a C_{60} cluster will remain self-assembled even if the confining domain is removed. Above said, programmable molecular packing in an arbitrary geometry can be achieved by a self-assembly process of the molecules in a confining domain of desirable geometry, and followed by transferring the patterned molecular cluster to the final designated location (e.g., another substrate).

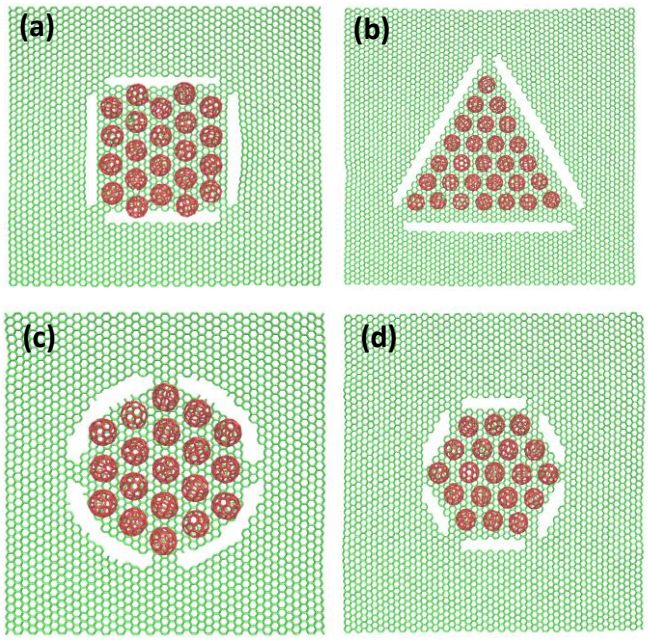

Figure 4.4 Domains of different shapes, e.g., (a) square, (b) triangular, (c) circular, and (d) hexagonal, can be generated in graphene to pattern C_{60}s into a cluster of designated geometry.

4.3.3. C_{60} molecules patterned in large domain

Finally, we demonstrate the feasibility of forming a giant molecular cluster by self-assembling a large number of C_{60} molecules in a confining domain defined by open slits in a graphene sheet. Figure 4.5 shows a large square-shaped domain with a side length of 100 Å and slit width of 4 Å. A total of 90 C_{60} molecules can be patterned with a triangular lattice into a square-shaped cluster, which remains stable and moves as a whole under thermal fluctuation.

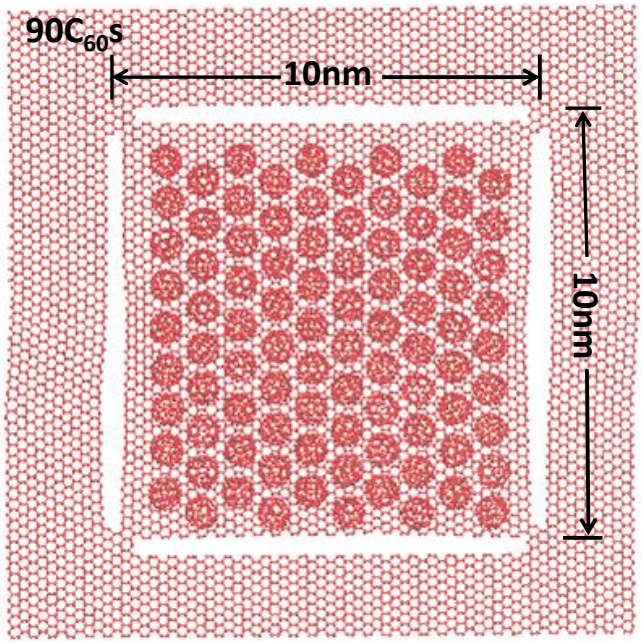

Figure 4.5 A large square-shaped confining domain with side length of 10 nm is generated in a graphene sheet, which can accommodate 90 C_{60}s densely packed into a triangular lattice as a giant molecular cluster.

4.4. Summary

In this Chapter, we reveal the "barrier effect" of an open slit in a graphene sheet, resulting from a net force pushing a molecule away as the molecule approaches the open slit. Such a barrier effect is nearly independent of the orientation of the open slit in the graphene sheet, therefore a molecule-confining domain of desirable shape can be readily created by simply introducing open slits that demarcate the domain. These appealing features can enable molecular self-assembly into an arbitrary geometry, a desirable but hard-to-achieve nanofabrication strategy. As a benchmark, we demonstrate that C_{60} molecules can self-assembly into stable clusters of various shapes and sizes inside confining domains enclosed by open slits in a graphene sheet.

Given that the barrier effect of an open slit is essentially due to a net vdW force acting on a molecule near the slit, it is expected the line-defect enabled molecular patterning on graphene demonstrated in the present work should be applicable to other material systems, such as nanoparticles and DNA. In this sense, the present findings shed light on a potential approach for molecular storage and patterning at nanoscale.

Chapter 5: Hydrogenation Enabled Nanostructure for Molecular Mass Manipulation

Hydrogenation has emerged as an effective way to modify graphene's morphology due to graphene's amendable surface chemistry feature. This Chapter studies novel hydrogenation enabled structure designed to serve specific molecular mass manipulation function. In Section 5.1, the concept of hydrogenation is briefly introduced. In section 5.2, a hydrogenated graphene bilayer structure for hydrogen storage and release is proposed. The key step for the development of a reliable hydrogen-based technology requires solving the issue of storage and transport of hydrogen. A novel structure which allows reversible mass uptake and release thus is desirable. Using molecular dynamics simulation, we show a partially hydrogenated bilayer graphene structure will serve this end. Simulation results show this kind of structure can adopt a tunnel shape which provides large space for hydrogen storage. To release the hydrogen, a displacement loading at two ends can lead to a transport efficiency as high as 82.3%. In Section 5.3, hydrogenation enabled nanofluidics system is studied. Carbon based materials have been extensively explored for the use of potential nanofluidic channels. While the existing structures such as carbon nanotube and graphene bilayer have a relatively simple geometry, a strategy to make complex channel network is highly desirable. In this Section, using molecular dynamics simulation, we show by patterning hydrogenation stripes in pristine graphene, channel of pre-defined shape can spontaneously form. Simulation results from a single straight channel as basic building block to a channel network with four

junctions are presented. As a demonstration, hydrogen flow conducted in such a channel network is also illustrated. The findings are summarized in section 5.4.

5.1. Hydrogenation of Graphene

Due to graphene's amendable surface chemistry feature, chemical functionalization is a promising approach to change the morphology of graphene. Tremendous efforts have been placed on the functionalization of pristine graphene by chemically adsorbing foreign atoms, molecules and functional groups of various types on its surface [117-123], motivated by the great potential of controllably tailoring the morphology of graphene. In particular, hydrogenation of graphene has been extensively explored. Hydrogenation is a process that involves bonding hydrogen atoms to carbon atoms in pristine graphene [117, 125]. The hybridization of graphene thus will be changed from sp^2 into sp^3 due to this chemical bonding. This process also gives rise to a local structural change around that carbon atom. Specifically, the chemically adsorbed hydrogen atom attracts the carbon atom it bonded with at the same time repels other neighboring carbon atoms. As a result, the three initially planar carbon-carbon bonds tend to bend away from the hydrogen atom, thus are distorted [126]. If hydrogen atoms are chemically adsorbed by the carbon atoms in pristine graphene on both its sides in an alternative manner, the resulting hydrogenated graphene (termed as graphane [117]) overall remains planar as the local out-of-plane distortion of the C-C bonds in each side cancel each other. If the graphene is single sided hydrogenated however, the local distortion at each

hydrogenated carbon atom accumulates and large out-of-plane deformation can be generated if sufficient carbon atoms in the graphene are hydrogenated on one side. The graphene morphology thus can be altered in a manner curving toward another side. Recently significant progress has been achieved on controllable hydrogenation of graphene. For example, single-sided hydrogenation of pristine graphene has been experimentally achieved [117, 119, 127-130].Recent studies show that hydrogen chemisorption in graphene can be enhanced by increasing local curvature of the carbon surface [131]. These progresses on programmable hydrogenation of graphene open up new pathways to controlling the morphology of graphene and therefore enable the exploration of graphene-based novel nanomaterials, which makes the proposed hydrogenated enabled structures in this paper feasible to achieve in experiments.

5.2. Molecular Mass Storage and Release Enabled by Hydrogenated Bilayer Graphene Structure

5.2.1. Background

Hydrogen is currently considered one of the most promising green fuels. The issue of finding systems and materials for efficient hydrogen storage is of great importance because it is the key enabling technology for realization of hydrogen energy economy. To offer a guidance on this goal, the Department of Energy (DOE) has established a target of 7.5% gravimetric density for hydrogen storage by the year 2017. In recent research, novel graphene based nanostructures have been proposed as

promising media for hydrogen storage because their extraordinary properties. For example, pillared graphene, a three-dimensional porous nanostructure has been proposed because that their large surface area will enable enlarged storage capability [115]. Giant fullerenes have also been explored to serve as a medium of high density hydrogen storage [116].

The above mentioned structures, however, suffered from two major limitations. First, the structure itself is complex and it remains unclear how to fabricate such a three-dimensional structure in a controlled manner. Secondly, after achieving mass storage, the associated mass transportation mechanism is not optimized. The closed nature of fullerene pose intrinsic challenge to uptake and release hydrogen, bond breaking is unavoidable which makes the mass uptake and release process irreversible. Therefore a novel structure which is easy to obtain and provides reversible hydrogen uptake and release is highly desirable.

To address this challenge, in this Section, we propose a novel partially hydrogenated bilayer graphene structure for hydrogen storage. Using molecular dynamics (MD) simulation we demonstrate that, our proposed structure is feasible to obtain. Also hydrogen release can be achieved by simply straining the bilayer structure which only involves the elastic deformation and therefore will not destroy the original structure. Thus the mass uptake and release is totally reversible.

5.2.2. Hydrogenation enabled graphene bilayer opening

In this section, we use MD simulation to demonstrate hydrogen assisted graphene bilayer opening up in which initially parallel, planar bilayer can be separated, leaving a space for future hydrogen molecules uptake.

Figure5.1 depicts the simulation model. A bilayer graphene of length 300 Å and width 30 Å is considered. For each layer, the single-sided hydrogenated stripe has a length of 100 Å. Periodic boundary condition is used in the width direction. In each carbon hexagon in the hydrogenated region, one hydrogen atom is chemically bonded to each of the three carbons in alternatively lattice positions. Therefore, half of the carbon atoms in the hydrogenated region are bonded with hydrogen atoms on the same side. In the simulation, the C-C and C-H bond as well as non-bonded C-C and C-H interactions are described by AIREBO potential. MD simulation is carried out using LAMMPS with Canonical Ensemble at a temperature of 300K. Before running dynamic simulations, the energy of the system is first minimized by using conjugate gradient (CG) algorithm until either the total energy change between successive iterations divided by the energy magnitude is less than or equal to 10-6 or the total force is less than 10-5 eV/ Å. Figure 5.2 plots the sequential snapshot of tunnel formation process. At the beginning of the simulation, we relax the bilayer structure by moving two ends towards center for 20 Å to allow the delamination morphology to occur.

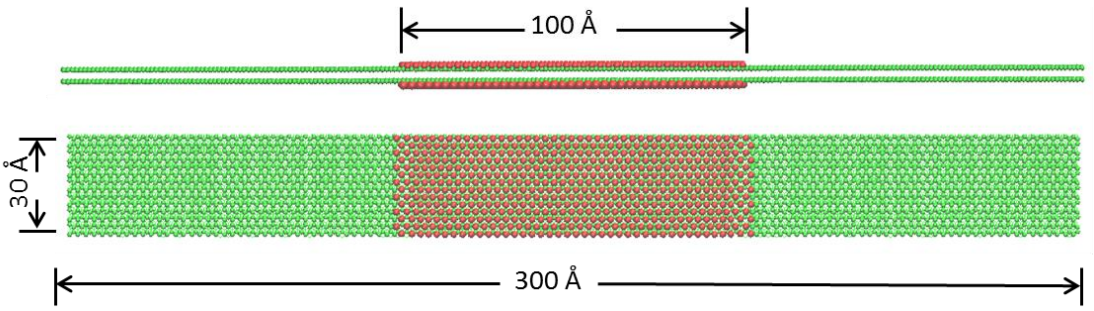

Figure 5.1 Side view and top view of the computation model. Basal graphene sheets have a length of 300 Å and a width 30 Å, they are both single-sided hydrogenated for a length of 100 Å. Red denotes the hydrogen atoms.

As shows in Figure 5.2, a small portion of the graphene layer bulge out at the edge of hydrogenated stripe. Driven by the hydrogenation induced local lattice distortion, the bulged out parts continue to extend and propagate towards center. During this process, the graphene sheets detach from each other. At t=20ps, the hydrogenated part has been entirely opened up, forming a tunnel shape. Under the effect of hydrogenation, the curved part will remain stable to release the strain energy, and the flat portion is adhered by inter-layer van der Waals force.

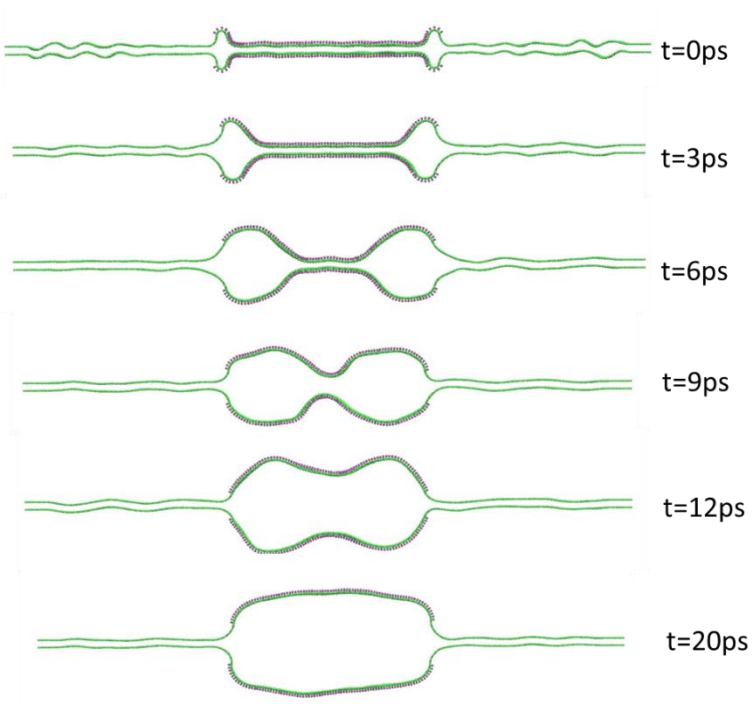

Figure 5.2 Sequential snapshots of the bilayer opening process enabled by hydrogenation. Driven by the hydrogenation induced local lattice distortion, the hydrogenated portions detach from each other and form a tunnel shape.

By applying the same strategy, different sizes of tunnels can be made by controlling the hydrogenation width. Figure 5.3 shows tunnel made of same basal graphene sheets but with different hydrogenated length of 25 Å, 50 Å, 75 Å and 100 Å respectively. As can be seen from the figure, the four corners have a same shape, while the increased hydrogenation length will increase the flat part. The final tunnel shape area is 790, 1720, 2720, 4370 $Å^2$ respectively.

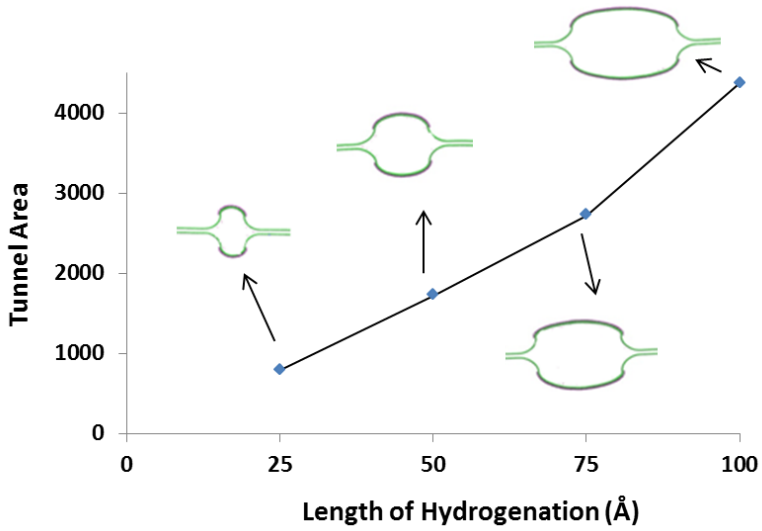

Figure 5.3 Tunnel shape and area as a function of hydrogenation length.

5.2.3. Hydrogen storage

Next we investigate the hydrogen storage capacity for the bilayer structure. For the basal graphene have a 30 Å depth and a 100 Å hydrogenation width, 8228 hydrogen atoms can be hosted within the opened space at a temperature of 70K. Due to the attractive vdW force between carbon atoms and hydrogen molecules, the hydrogen molecules can stabilize within the volume. If more hydrogen molecules are stuffed, the increased pressure can overcome the vdW adhesion between bilayer graphene and cause a delamination. Therefore the total number of hydrogen molecules will be a function of the delamination length. As the first column in figure 5.4 shows, when 12584 hydrogen atoms occupy in the bilayer structure, an additional 12 Å graphene bilayer is delaminated. A further delamination of 12 Å will lead to an ultimate capacity of 16456 atoms. A complete table of number of hydrogen molecules for bilayer structures of different hydrogenation width and delamination length is

listed in figure 5.4. This serves as a guide to predict the ultimate capacity of the bilayer structures of different sizes and delamination length.

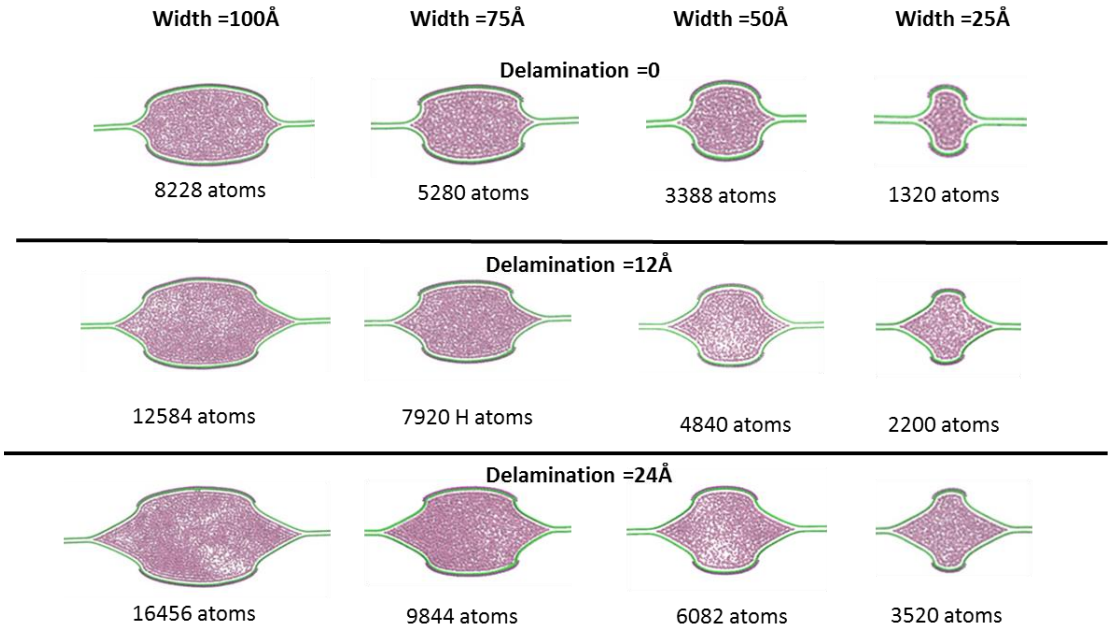

Figure 5.4 A complete table of total hydrogen atoms stored in the bilayer structure as a function of hydrogenation width and the delamination length.

5.2.4. Mass release by displacement loading

The release of hydrogen molecules is investigated. The starting structure is a bilayer structure consists of basal graphene sheets with length of 200 Å, depth of 150 Å and a hydrogenation width of 75 Å. 8734 hydrogen molecules are initially inside the structures. A displacement load is applied by gradually stretching the two ends of the bilayer at 0.1 Å/fs. To allow the hydrogen to escape, the periodical boundary is modified (the box size along tunnel direction increases a little bit) so that the tunnel is no longer seamless at the boundary. The evolution of the amount of the adsorbed

hydrogen molecules remaining inside the CNS is presented as a function of the applied tensile deformation. Initial deformation causes the tightening of the opening bilayer structure, reducing the cross section area, which in turn imposes a stronger repulsive vdW force on the hydrogen molecules. As a result, some hydrogen molecules are pushed out of the graphene bilayer. Upon further application of the displacement loading, the bilayer structure flattens when the displacement of the two ends reaches 20 Å. At this stage, the graphene sheets almost have zero strain and 50% of the adsorbed hydrogen molecules are squeezed out. As the displacement loading further increases and graphene sheets begin to experience strain, much more adsorbed hydrogen molecules are transported however with a slower rate as indicated by a more gradual slope of the curve in Figure 5.5. Given the high deformability of the basal graphene sheet, a total displacement of 60 Å, which is equivalent to 20% strain, can be applied to the bilayer graphene. At the end of the loading, 82.3% of the hydrogen molecules initially adsorbed are squeezed out of the bilayer, suggesting the high efficacy of the molecular transport.

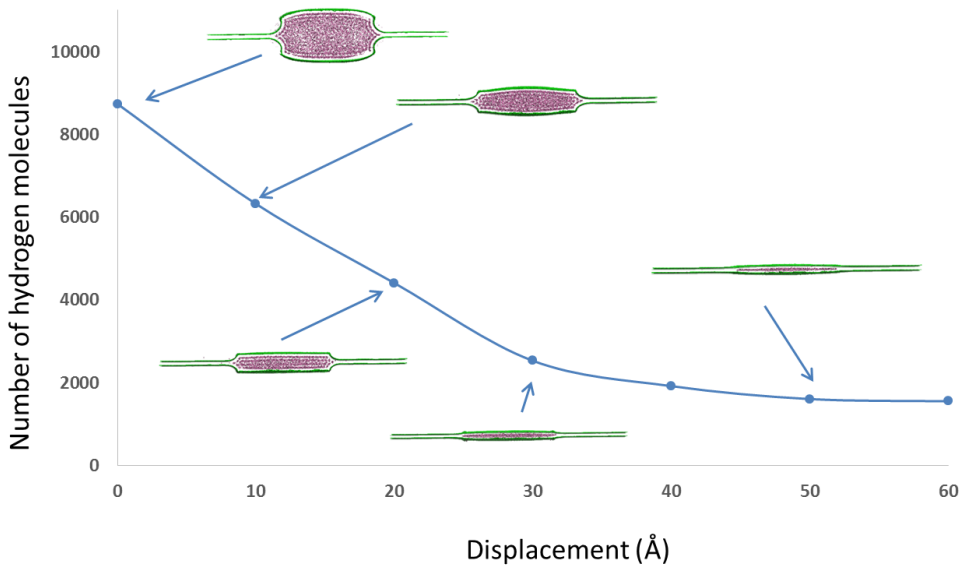

Figure 5.5 Number of hydrogen molecules remaining inside the bilayer structure as a function of the displacement of the two ends. At the end of the loading, 82.3% of the hydrogen molecules initially adsorbed are squeezed out of the bilayer

5.3. Hydrogenation Enabled Nanofluidic Channel

5.3.1. Background

Nanofluidics has been studied extensively in recent years for their unique properties that are very distinct from macroscopic fluidic systems [131]. In particular, nanofluidic phenomena in carbon-based materials are of great interest because carbon material's smooth hydrophobic graphitic walls will facilitate ultrafast nanoflow [132-134]. A variety of carbon-based nanofluidic devices have been proposed. For instance, carbon nanotube has been used to conduct water and gas molecules in which ultra-efficient flow was observed [132]. Carbon nanoscroll has been used as tunable water channel. Bilayer graphene has also been studied as two dimensional

nanofluidics [135]. These studies of nanofluidic channel will have profound implication such as water desalination, water purification, nanofiltration, drug delivery and so on.

While the previous carbon-based nanochannel provide a platform for fundamental studies of nanofluidics, most of them have the limitation that they have a relatively simple geometry, such as one dimensional nanotube and nano-channels or two dimensional bilayer graphene structure. Also these structures with uniform geometry do not have a selective feature. Therefore, a nanofluidic platform with a complex geometry to conduct multi-directional and selective nanoflow will be highly desirable. To address this challenge, in this study, we propose a simple but novel strategy that uses patterned hydrogenation on graphene sheet to enable spontaneous multi-directional nanofluidic channel formation.

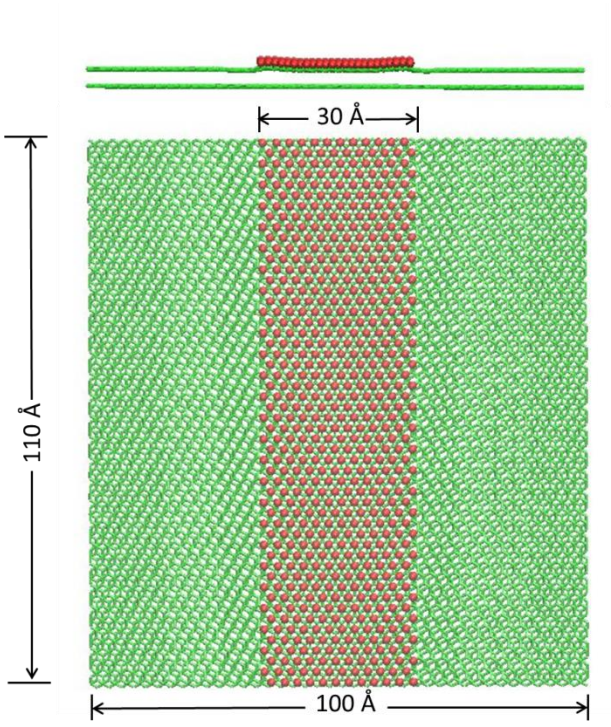

Figure 5.6 Side view and top view of the computation model. Basal graphene sheet has a length of 100 Å and a width of 110 Å. The single-sided hydrogenated strip has a width of 30 Å. Red denotes the hydrogen atoms.

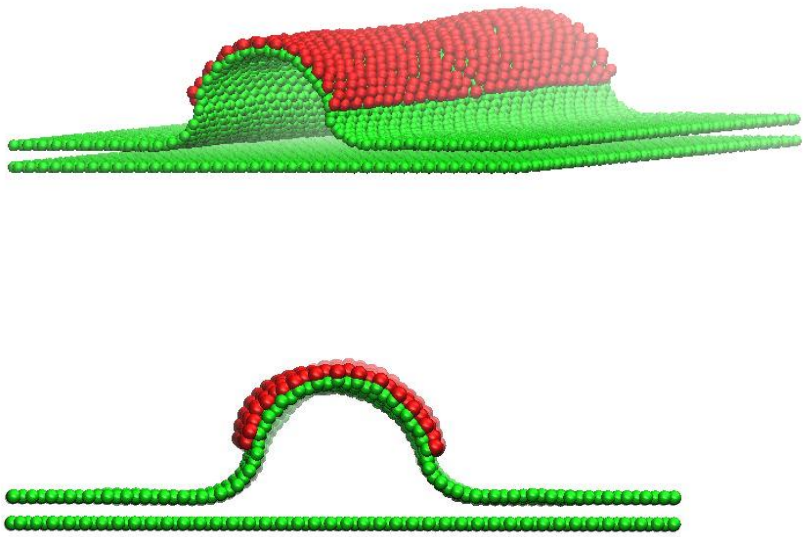

Figure 5.7 Hydrogenated strip detaches from supporting layer and form a channel.

5.3.2. Hydrogenation enabled channel formation

In this section we first demonstrate spontaneous channel formation enabled by patterning a rectangular hydrogenation stripe, which serves as the fundamental building block in nanofluidic channel network. Figure5.6 depicts the simulation model. A partially hydrogenated graphene is supported on some certain substrates. To simplify the simulation however, we represent the substrate by fixing a pristine graphene sheet in the bottom. The graphene sheet is of length 100 Å and width 110 Å.

Periodic boundary condition is used in the width direction. The hydrogenated stripe has a width of 30Å. In each carbon hexagon in the hydrogenated region, one hydrogen atom is chemically bonded to each of the three carbons in alternatively lattice positions. Therefore, half of the carbon atoms in the hydrogenated region are bonded with hydrogen atoms on the same side. In the simulation, the C-C and C-H bond as well as non-bonded C-C and C-H interactions are described by AIREBO potential. MD simulation is carried out using LAMMPS with Canonical Ensemble at a temperature of 77K. Before running dynamic simulations, the energy of the system is first minimized by using conjugate gradient (CG) algorithm until either the total energy change between successive iterations divided by the energy magnitude is less than or equal to 10-6 or the total force is less than 10-5 eV/ Å. At the beginning of the simulation, we relax the structure by moving two ends towards center for 15 Å. Driven by the hydrogenation induced local lattice distortion, the hydrogenated part immediately detaches from the supporting layer, and form a channel spontaneously as Figure 5.7 shows. It's demonstrated from this simulation that straight tunnel can be formed according to the patterns of hydrogenation stripe. This can be regarded as building blocks for more complex channel system, and it's envisioned that, by appropriately patterning hydrogenation stripe on graphene, more complex channel systems can be made in a similar manner.

5.3.3. Channel with junction

With the understanding of a single straight channel, we now turn to investigate a more complex pattern: two channels with junction in the center. In this

computation model as shows in figure 5.8, the square shaped graphene has a side length of 185 Å. The two hydrogenation stripe both has a width of 30 Å. Periodic boundary condition is used in both directions.

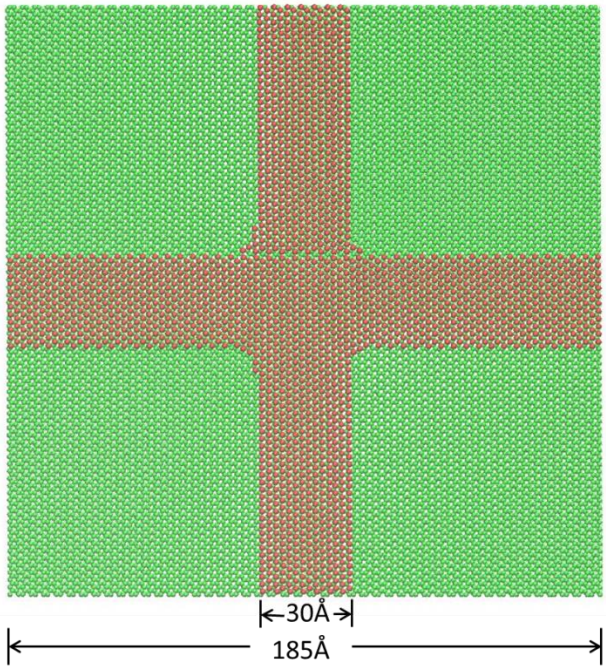

Figure 5.8 Top view of the computation model. Basal graphene sheet has a side length of 185 Å. The two single-sided hydrogenated strip has a width of 30 Å. Red denotes the hydrogen atoms.

In this case, a biaxial compression with an amplitude of 15 Å is applied to facilitate the tunnel formation. After compression, the two stripes bulge out, forming a two way continuous channel with an X-junction as figure 5.9 shows. Due to the compression, there are also several kinks along the channel.

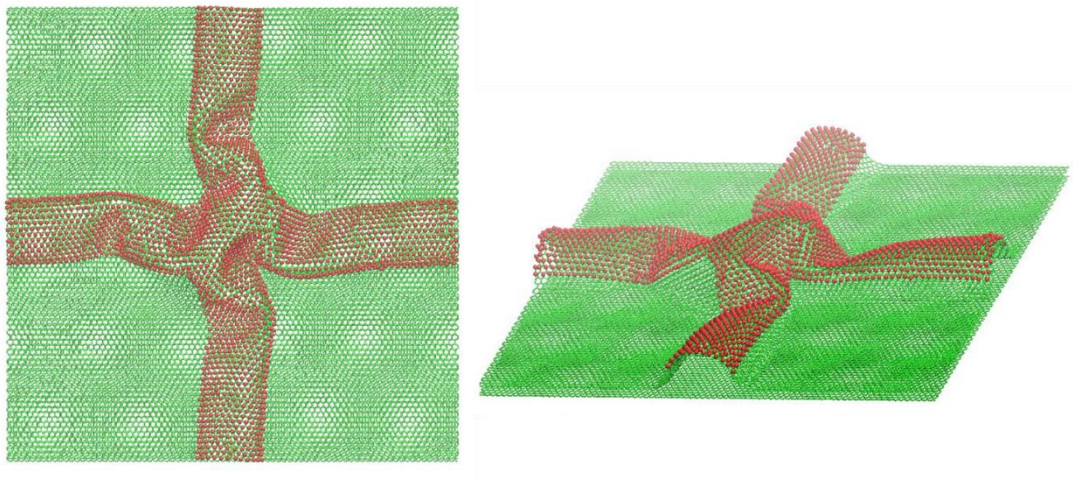

Figure 5.9 Channel with junction spontaneously formed after biaxial compression enabled by two stripes of hydrogenation.

With this continuous channels with junction, it's envisioned that two directional nanoflow can be conducted through this kind of channel network.

5.3.4. Channel network

As a demonstration, in this section, we demonstrate flow of hydrogen molecules can be conducted in a channel network enabled by hydrogenation stripes. The channel network consists of four junctions in last section. Hydrogen source is provided from the two channel entrances on the right. As figure 5.10 shows, hydrogen molecules enter from the right entrances and after they reach the junction, they diverge to three directions. Eventually, hydrogen molecules exit from other six outlets. This simulation demonstrates that this proposed channel network enabled by patterning hydrogenation can effectively conduct multi-directional nanoflow.

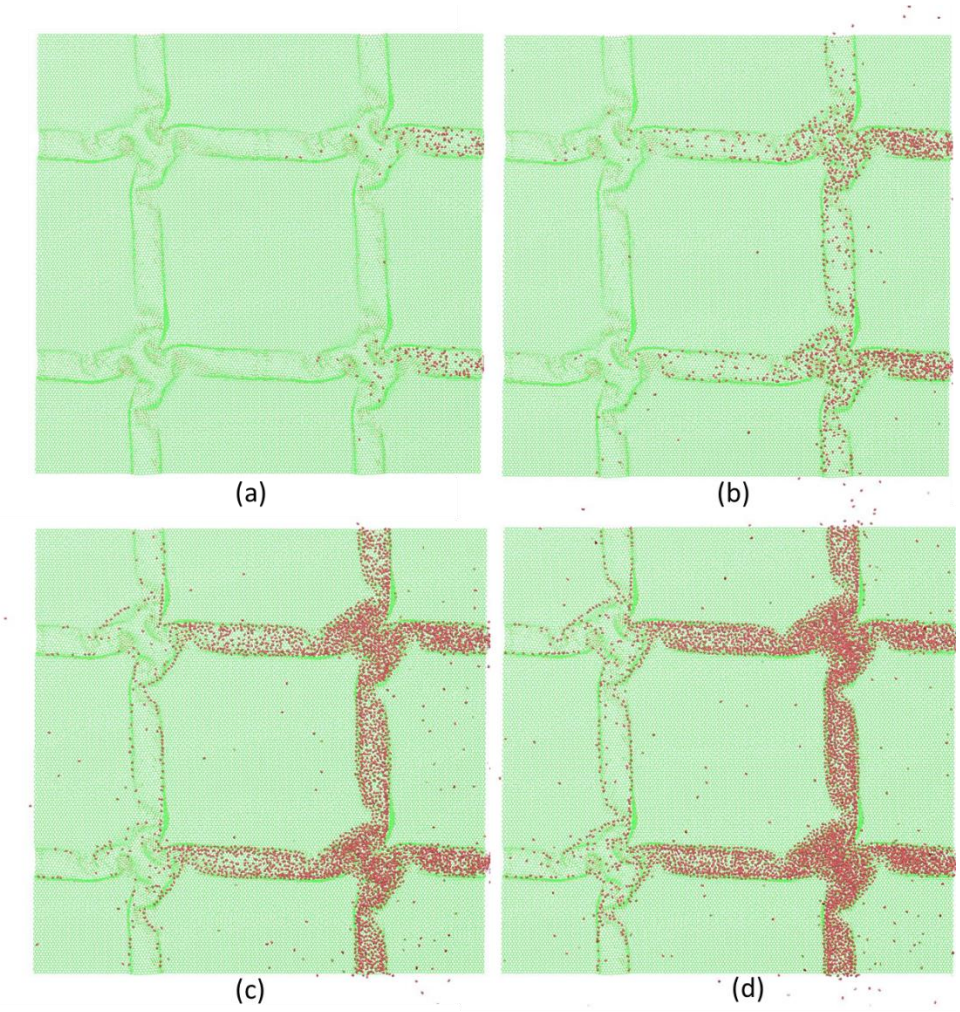

Figure 5.10 Hydrogen molecules flow in the channel network. Hydrogen flux is provided from the channel entrance on the right side. For visual clarity, the bottom layer is not shown here.

5.3.5. Channel with changing cross section area

The previous nanofluidic channel systems have a uniform geometry feature, which is a limitation to conduct selective nanoflow. For example, it's desirable for a nanofluidic channel to separate small molecules from a mixture of particles of various sizes. The above mentioned hydrogenation enabled channel formation will serve this

end. By patterning pre-defined hydrogenation shape on pristine graphene sheet, channel with varying cross section area can be feasibly made.

Figure 5.11 show the simulation model. Periodic boundary condition is used in horizontal direction. To initiate the channel formation, a compression of 15 Å is applied, followed by hydrogenated part bulging out and forming a funnel shaped channel. This channel has the largest cross section at one end, and gradually becomes smaller towards the other end as shows in figure 5.12.

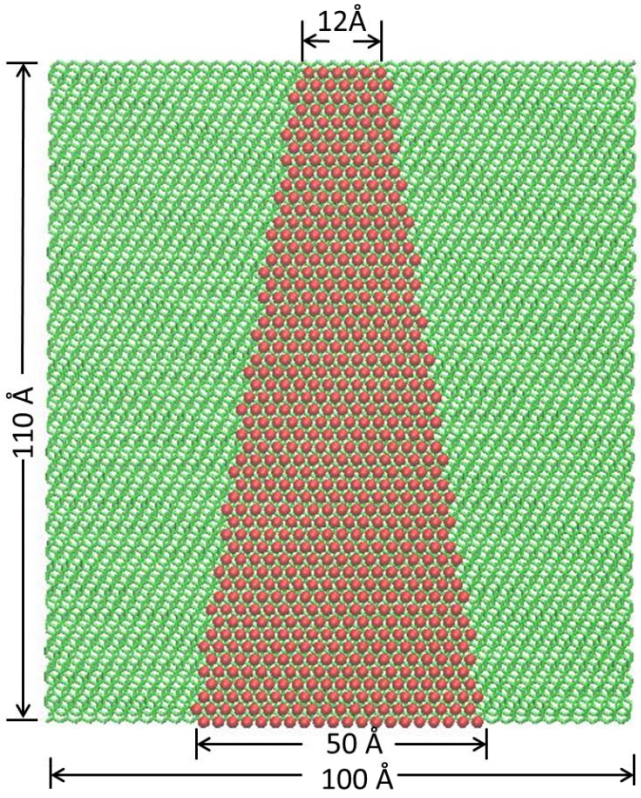

Figure 5.11 Top view of the computation model. Red denotes hydrogen atoms.

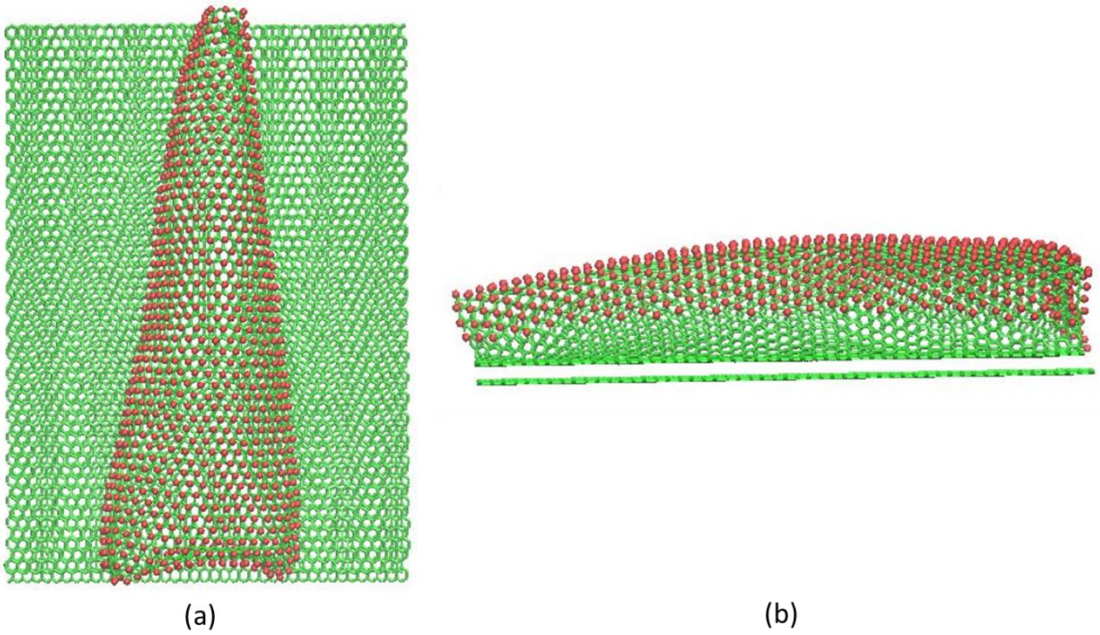

Figure 5.12 (a) Top view and (b) side view of the funnel shaped tunnel.

To demonstrate the selective feature of the funnel shaped channel, a mixture of hydrogen molecules and a C_{60} are initially inside the channel. The C_{60} molecule has a much larger size than that of hydrogen molecules. Figure 5.13 illustrates the filtering process. A virtual wall is used to push the molecules towards the smaller end. As the molecules aggregate near the end, hydrogen molecules are pushed out of the channel because of their smaller sizes while the C_{60} remains inside. This example clearly shows that a channel with a changing geometry can conduct nanoflow selectively, by separating molecules of different sizes. This may find various of potential applications such as nanofiltration.

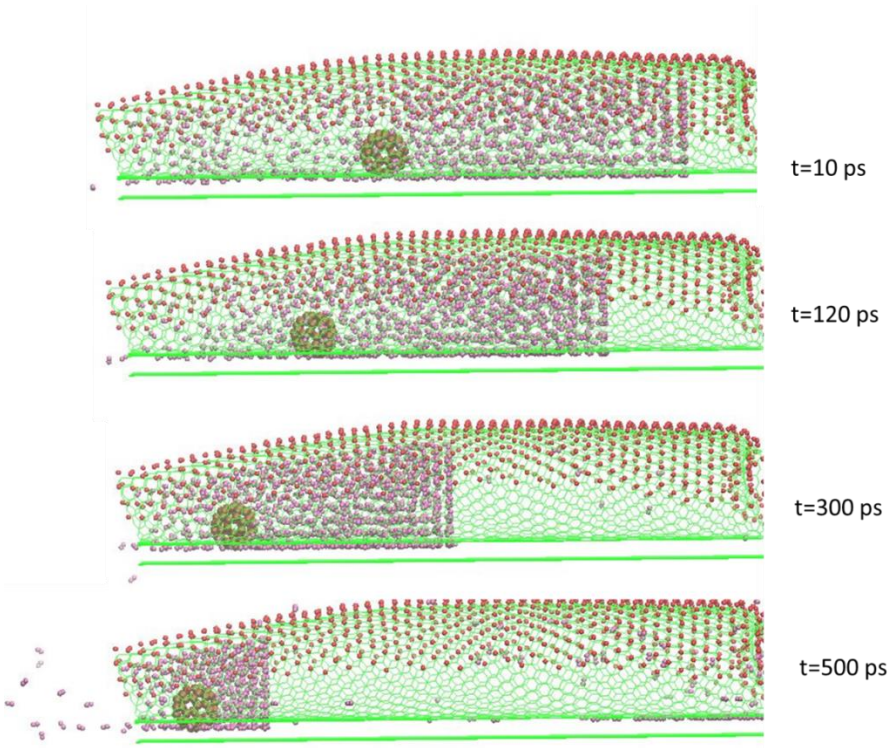

Figure 5.13 Illustration of the selective feature of the funnel shaped channel. Initially a mixture of hydrogen atoms and a C_{60} are placed inside the channel. A virtual wall is used to push them towards the smaller end. As they arrive near the end, the hydrogen molecules are pushed out of the channel while the C_{60} remains inside.

5.4. Summary

In summary, we proposed novel hydrogenation-assisted graphene structures for molecular mass manipulation use. Theories and experiments have demonstrated that hydrogenation is an effective way to tune the morphology of graphene, which is also proved in our simulation study.

First we studied hydrogenation enabled bilayer graphene opening. Using molecular dynamics simulations, we demonstrate this kind of structure has large

capacity to accommodate hydrogen molecules. The ultimate capacity can be further increased by additional delamination of the graphene bilayer while the whole structure remaining stable. The mass release mechanism associated with this structure is quite straightforward. By applying tensile loading at the two ends, a high efficacy of hydrogen molecule transportation up to about 82.3% can be achieved. The advantage of this transport method is that it doesn't damage the original material. The structure can be recovered upon unloading given the high elastic deformability of graphene. Therefore the mass uptake and release is totally reversible. As the mass storage and transport mechanism demonstrated in this paper are essentially driven by the non-bonded interaction of the hydrogen molecules and the basal graphene sheets, it is expected that the similar mechanisms are applicable for molecular mass of other types, such as water molecules, DNAs, fullerenes, and nanoparticles.

Following this idea, we also proposed a novel strategy to precisely control the shape of nanofluidic channel. This method use patterned hydrogenation to induce spontaneous channel formation. This idea provides a design principle to robustly obtain a variety of geometries including one-dimensional straight channel, channel networks, and funnel shaped channel. Simulations show that the self-assembled network is stable and can conduct hydrogen flow in multiple directions. And the funnel shaped channel is able to separate large sized molecules from a mixture of particles. With the advance in hydrogenation technics, it's envisioned that channel network with more complicated shapes and junctions can be made by precisely designing and patterning the hydrogenation.

Chapter 6: Summary and Future Work

6.1. Summery and Concluding Remarks

This dissertation attempts to explore the novel graphene based structures and their associated mass manipulation mechanism to achieve mass transportation, patterning, and storage in a controllable and programmable fashion. The main research findings and scientific contributions of this dissertation are listed as follows:

Contribution 1: Two strategies to achieve molecular mass transportation through CNS have been found. One is through torsional buckling induced instability of CNS. It's found that a lower loading rate will result in a higher transportation efficiency because with a more gradual buckling deformation the vdW force between molecules and carbon atoms will play a more effective role. Overall, the transportation mechanism is effective in a wide range of loading rate. The second mechanism is enabled by surface energy induced radial shrinking. It's showed that the larger the change in the surface energy of basal graphene, the better the hydrogen molecule transportation efficiency.

Contribution 2: A fundamental law of directional transport of molecular mass by straining is found. A strain gradient in basal graphene can generate a net transport force because of the broken symmetry of the atoms distribution. Simulations show that various type of molecular mass can be transported through this mechanism including carbon nanotube, gold particle, graphene flakes and fullerenes. In particular,

graphene flakes and carbon nanotubes can be used as vehicles to carry other molecular mass.

Contribution 3: A barrier effect of line defects in graphene is revealed which can potentially enable molecular confining and patterning in a domain of desirable geometry. The missing carbon atoms at the slit result in a net vdW force acting on the molecules in the direction perpendicular to the slit and pointing to the direction away from the slit. Simulations show that fullerene molecules can be readily patterned into a stable cluster of various shapes and sizes. Such a strategy is expected to be applicable to pattern various types of molecules that interact with graphene via vdW force.

Contribution 4: A partially hydrogenated bilayer graphene structure is found to be adopting a tunnel shape under the lattice distortion effect of hydrogenation. This opens a space for hydrogen storage and the ultimate capacity is related to the width of hydrogenation and the delamination of the original graphene bilayer. The mass release mechanism associated is simply to stretch the bilayer structure. Due to large deformability of graphene, the whole mass uptake and release process is non-damageable and reversible.

Contribution 5: Proposed a novel method to fabricated complex nanofluidic channel. By patterning the hydrogenation stripes on pristine graphene, channel network of pre-defined geometry can be spontaneously formed. This idea provides a design principle to robustly obtain a variety of geometries including one-dimensional

straight channel, channel networks, and funnel shaped channel. Simulations show that the self-assembled network is stable and can conduct hydrogen flow in multiple directions. And the funnel shaped channel is able to separate large sized molecules from a mixture of particles.

6.2. Future Work

Beyond the work in this dissertation, the following works can be further explored.

6.2.1. Straining induced vdW force change and its effect on mass transportation

In the study of directional transportation of molecular mass by straining graphene, graphene is supposed to be stretched as much as 20% in the maximum strain end. The existing study treats the vdW interaction uniform across the basal graphene, which is not true in some conditions. Such a large strain will in fact cause the polarization of the carbon atoms which in turn affects the vdW interaction. Therefore, the coefficient of vdW force should be strain dependent thus will vary from place to place. Accordingly the strength of transportation force will be affected. A more accurate model that captures this effect is interesting to study.

6.2.2. Generation of strain gradient in graphene by experiment method

With the prediction by molecular dynamics simulation, it's interesting to explore experiment method to verify the results. However some simulation condition is very difficult to achieve with current experiment techniques. Therefore it's

important to find other alternative methods that are more feasible to realize in experiment condition. For example, as studied in Chapter 3, strain gradient in graphene sheet can lead to directional mass transport, however it still remain unclear that how to apply such a complex loading to graphene sheet in experiment. An alternative way to do this is to apply a uniform load to a graphene sheet with varying modulus. Hydrogenated graphene which is known as graphane and is feasible to achieve in experiments, has a lower Young's modulus than graphene. By patterning hydrogenation with a pre-defined shape on graphene sheet, this hybrid material can be designed to have varying modulus that strain gradient can be generated by applying uniaxial stretching to it.

Bibliography

[1] A. K. Geim and K. S. Novoselov, "The rise of graphene," *Nat Mater,* vol. 6, pp. 183-191, 2007.

[2] J. C. Meyer, A. K. Geim, M. I. Katsnelson, K. S. Novoselov, T. J. Booth, and S. Roth, "The structure of suspended graphene sheets," *Nature,* vol. 446, pp. 60-63, 2007.

[3] K. S. Novoselov, A. K. Geim, S. V. Morozov, D. Jiang, Y. Zhang, S. V. Dubonos, I. V. Grigorieva, and A. A. Firsov, "Electric Field Effect in Atomically Thin Carbon Films," *Science,* vol. 306, pp. 666-669, 2004.

[4] Y. B. Zhang, Y. W. Tan, H. L. Stormer, and P. Kim, "Experimental observation of the quantum Hall effect and Berry's phase in graphene," *Nature,* vol. 438, pp. 201-204, Nov 2005.

[5] http://nobelprize.org/nobel_prizes/physics/laureates/2010.

[6] A. K. Geim and P. Kim, "Carbon wonderland," *Scientific American,* vol. 298, pp. 90-97, Apr 2008.

[7] X. S. Li, W. W. Cai, J. H. An, S. Kim, J. Nah, D. X. Yang, R. Piner, A. Velamakanni, I. Jung, E. Tutuc, S. K. Banerjee, L. Colombo, and R. S. Ruoff, "Large-Area Synthesis of High-Quality and Uniform Graphene Films on Copper Foils," *Science,* vol. 324, pp. 1312-1314, 2009.

[8] P. W. Sutter, J. I. Flege, and E. A. Sutter, "Epitaxial graphene on ruthenium," *Nature Materials,* vol. 7, pp. 406-411, May 2008.

[9] K. S. Kim, Y. Zhao, H. Jang, S. Y. Lee, J. M. Kim, K. S. Kim, J.-H. Ahn, P. Kim, J.-Y. Choi, and B. H. Hong, "Large-scale pattern growth of graphene films for stretchable transparent electrodes," *Nature,* vol. 457, pp. 706-710, 2009.

[10] A. Reina, X. T. Jia, J. Ho, D. Nezich, H. B. Son, V. Bulovic, M. S. Dresselhaus, and J. Kong, "Large Area, Few-Layer Graphene Films on Arbitrary Substrates by Chemical Vapor Deposition," *Nano Letters,* vol. 9, pp. 30-35, Jan 2009.

[11] G. Eda, G. Fanchini, and M. Chhowalla, "Large-area ultrathin films of reduced graphene oxide as a transparent and flexible electronic material," *Nat Nano,* vol. 3, pp. 270-274, 2008.

[12] C. Berger, Z. M. Song, X. B. Li, X. S. Wu, N. Brown, C. Naud, D. Mayou, T. B. Li, J. Hass, A. N. Marchenkov, E. H. Conrad, P. N. First, and W. A. de Heer, "Electronic confinement and coherence in patterned epitaxial graphene," *Science,* vol. 312, pp. 1191-1196, 2006.

[13] Ultimate Permeation Across Atomically Thin Porous Graphene

[14] C. Lee, X. Wei, J. W. Kysar, and J. Hone, "Measurement of the Elastic Properties and Intrinsic Strength of Monolayer Graphene," *Science*, vol. 321, pp. 385-388, 2008.

[15] Q. Lu, and R. Huang, "Effect of edge structures on elastic modulus and fracture of graphene nanoribbons under uniaxial tension," *rXiv:1007.3298v1*

[16] R. Murali, K. Brenner, Y. X. Yang, T. Beck, and J. D. Meindl, "Resistivity of Graphene Nanoribbon Interconnects," *Ieee Electron Device Letters*, vol. 30, pp. 611-613, 2009.

[17] S. V. Morozov, K. S. Novoselov, F. Schedin, D. Jiang, A. A. Firsov, and A. K. Geim, "Two-dimensional electron and hole gases at the surface of graphite," *Physical Review B*, vol. 72, 2005.

[18] J. H. Chen, C. Jang, S. D. Xiao, M. Ishigami, and M. S. Fuhrer, "Intrinsic and extrinsic performance limits of graphene devices on SiO2," *Nature Nanotechnology*, vol. 3, pp. 206-209, 2008.

[19] R. R. Nair, P. Blake, A. N. Grigorenko, K. S. Novoselov, T. J. Booth, T. Stauber, N. M. R. Peres, and A. K. Geim, "Fine structure constant defines visual transparency of graphene," *Science*, vol. 320, pp. 1308-1308, 2008.

[20] I. Jung, M. Pelton, R. Piner, D. A. Dikin, S. Stankovich, S. Watcharotone, M. Hausner, and R. S. Ruoff, "Simple approach for high-contrast optical imaging

and characterization of graphene-based sheets," *Nano Letters,* vol. 7, pp. 3569-3575, 2007.

[21] E. Stolyarova, K. T. Kwang, S. Ryu, J.Maultzsch, P. Kim, L. Brus, T. Heinz, M. Hybertsen, G. Flynn "High-resolution scanning tunneling microscopy imaging of mesoscopic graphene sheets on an insulating surface." *Proceedings of the National Academy of Sciences of the United States of America* **104**, 9209-9212, 2007.

[22] P. Sessi, J. Guest, M. Bode, N. Guisinger, "Patterning graphene at the nanometer scale via hydrogen desorption." *Nano Letters* **9**, 4343-4347, 2009.

[23] S. Ryu *et al.*, "Reversible basal plane hydrogenation of graphene." *Nano Letters* **8**, 4597-4602, 2008.

[24] X. Wang, S. Tabakman, H. Dai, "Atomic layer deposition of metal oxides on pristine and functionalized graphene." *Journal of the American Chemical Society* **130**, 8152–8153, 2008.

[25] D. Boukhvalov, M. Katsnelson, "Chemical functionalization of graphene with defects." *Nano Letters* **8**, 4373-4379, 2008.

[26] D. Boukhvalov, M. Katsnelson, A. Lichtenstein, "Hydrogen on graphene: Electronic structure, total energy, structural distortions and magnetism from first-principles calculations." *Physical Review B* **77**, 035427, 2008.

[27] R. Balog, B. Jørgensen, L. Nilsson, M. Andersen, E. Rienks, M. Bianchi, M. Fanetti, E. Lægsgaard, A. Baraldi, S. Lizzit, Z. Sljivancanin, F. Besenbacher, B. Hammer, T. G. Pedersen, and P. Hofmann, "Bandgap opening in graphene induced by patterned hydrogen adsorption." *Nature Materials* **9**, 315-319, 2010.

[28] T. Kudernac, N. Ruangsupapichat, M. Parschau, B. Maciá, N. Katsonis, S. R. Harutyunyan, K. Ernst and B. L. Feringa, "Electrically driven directional motion of a four-wheeled molecule on a metal surface." *Nature* 479, 208-211, 2011.

[29] A. Barreiro, R. Rurali, E. R. Hernandez, J. Moser, T. Pichler, L. Forro, A. Bachtold, and R. Harutyunyan, "Subnanometer Motion of Cargoes Driven by Thermal Gradients Along Carbon Nanotubes." *Science* vol. 320, pp. 775-778, 2008.

[30] Braga, S. F., Coluci, V. R., Legoas, S. B., Giro, R., Galva˜o, D. S., and Baughman, R. H., "Structure and Dynamics of Carbon Nanoscrolls," *Nano Letters* 4(5), pp. 881–884 2004.

[31] Coluci, V. R., Braga, S. F., Baughman, R. H., and Galva˜o, D. S., "Prediction of the Hydrogen Storage Capacity of Carbon Nanoscrolls," *Physics Review B*, 75(12), p. 125404, 2007.

[32] Braga, S. F., Coluci, V. R., Baughman, R. H., and Galva˜o, D. S., 2007, "Hydrogen Storage in Carbon Nanoscrolls: An Atomistic Molecular Dynamics Study," *Chemistry Physics Letter*, 441(1–3), pp. 78–82, 2007.

[33] Mpourmpakis, G., Tylianakis, E., and Froudakis, G. E., "Carbon Nanoscrolls: A Promising Material for Hydrogen Storage," Nano Letter, 7(7), pp. 1893–1897, 2007.

[34] Shi, X., Pugno, N. M., Cheng, Y., and Gao, H., "Gigahertz Breathing Oscillators Based on Carbon Nanoscrolls," *Applied Physics Letter*, 95(16), p. 163113, 2009.

[35] Xie, X., Ju, L., Feng, X., Sun, Y., Zhou, R., Liu, K., Fan, S., Li, Q., and Jiang, K., "Controlled Fabrication of High-Quality Carbon Nanoscrolls From Monolayer Graphene," *Nano Letters*, 9(7), pp. 2565–2570, 2009.

[36] Shi, X., Cheng, Y., Pugno N. M., and Gao, H., "Tunable Water Channels With Carbon Nanoscrolls," *Small*, 6(6), pp. 739–744, 2009.

[37] Zhang, Z., and Li, T., "Carbon Nanotube Initiated Formation of Carbon Nanoscrolls," *Applied Physics Letter*, 97(8), p. 081909, 2010.

[38] Shi, X. H., Pugno, N. M., and Gao, H. J., "Mechanics of Carbon Nanoscrolls: A Review," *Acta Mech. Solida Sinica*, 23(6), pp. 484–497, 2010.

[39] Shi, X., Cheng, Y., Pugno, N. M., and Gao, H., "A Translational Nanoactuator Based on Carbon Nanoscrolls on Substrates," *Applied Physics Letter*, 96(5), p. 053115, 2010.

[40] Zhang, Z., and Li, T., "Ultrafast Nano-Oscillators Based on InterlayerBridged Carbon Nanoscrolls," *Nanoscale Research Letter*, 6, p. 470, 2011.

[41] Wang, Q., "Transportation of Hydrogen Molecules Using Carbon Nanotubes in Torsion," *Carbon*, 47(7), pp. 1870–1873, 2009.

[42] Wang, Q., "Atomic Transportation Via Carbon Nanotubes," *Nano Letters*, 9(1), pp. 245–249, 2009.

[43] Duan, W. H., and Wang, Q., "Water Transport With a Carbon Nanotube Pump," *ACS Nano*, 4(4), pp. 2338–2344, 2010.

[44] Wu, N., Wang, Q., and Arash, B., "Ejection of DNA Molecules From Carbon Nanotubes," *Carbon*, 50(13), pp. 4945–4952, 2012.

[45] Insepov, Z., Wolf, D., and Hassanein, A., "Nanopumping Using Carbon Nanotubes," *Nano Letters*, 6(9), pp. 1893–1895, 2006.

[46] Brenner, D. W., Shenderova, O. A., Harrison, J. A., Stuart, S. J., Ni, B., and Sinnott, S. B.,"A Second-Generation Reactive Empirical Bond Order (REBO)

Potential Energy Expression for Hydrocarbons," *Journal of Physics of Condens Matter*, 14(4), pp. 783–802, 2002.

[47] Stuart, S. J., Tutein, A. B., and Harrison, J. A., "A Reactive Potential for Hydrocarbons With Intermolecular Interactions," *Journal of Chemistry Physics*, 112(14), pp. 6472–6486, 2000.

[48] Gu, C., Gao, G. H., Yu, Y. X., and Mao, Z.-Q., "Simulation Study of Hydrogen Storage in Single Walled Carbon Nanotubes," *International Journal of Hydrogen Energy*, 26(7), pp. 691–696. 2001.

[49] Zhou, B., Guo, W. L., and Tang, C., "Chemisorption of Hydrogen Molecules on Carbon Nanotubes: Charging Effect From First-Principles Calculations," *Nanotechnology*, 19(7), p. 075707, 2008.

[50] Plimpton, S., "Fast Parallel Algorithms for Short-Range Molecular Dynamics," *Journal of Computational Physics*, 117(1), pp. 1–19, 1995.

[51] Zhang, Z., Huang, Y., and Li, T., "Buckling Instability of Carbon Nanoscrolls," Journal of Applied Physics, 112(6), p. 063515, 2012.

[52] Allen, M. P., and Tildesley, D. J., *Computer Simulation of Liquids*, Clarendon, Oxford, UK, 1987.

[53] Y. Shirai, A. Osgood, Y. Zhao, K. Kelly, J. Tour, "Directional control in thermally driven single-molecule nanocars," *Nano Letters* 5 2330–2334, 2005.

[54] T. Kudernac, N. Ruangsupapichat, M. Parschau, B. Macia, N. Katsonis, S. Harutyunyan, K. Ernst, B. Feringa, Electrically driven directional motion of a four-wheeled molecule on a metal surface, *Nature* 479 208–211, 2011.

[55] A. Barreiro, R. Rurali, E. Hernandez, J. Moser, T. Pichler, L. Forro, A. Bachtold, "Subnanometer motion of cargoes driven by thermal gradients along carbon nanotubes", *Science* 320 775–778, 2008.

[56] J. Holt, H. Park, Y. Wang, M. Stadermann, A. Artyukhin, C. Grigoropoulos, A. Noy, O. Bakajin, Fast mass transport through sub- 2-nanometer carbon nanotubes, *Science* 312 1034–1037, 2006.

[57] M. Whitby, N. Quirke, "Fluid flow in carbon nanotubes and nanopipes", *Nature Nanotechnology* 2 87–94, 2007.

[58] G. Whitesides, The origins and the future of microfluidics, *Nature* 442 368–373, 2006.

[59] H. Qiu, R. Shen, W. Guo, "Vibrating carbon nanotubes as water pumps", *Nano Research* 4 284–289, 2011.

[60] W. Duan, Q. Wang, "Water transport with a carbon nanotube pump", *ACS Nano* 4 2338–2344, 2010.

[61] X. Li, G. Kong, X. Zhang, G. He, "Pumping of water through carbon nanotubes by rotating electric field and rotating magnetic field", *Applied Physics Letters* 103 143117, 2013.

[62] Q. Xue, D. Xia, C. Lv, N. Jing, C. Ling, “Molecule delivery by the domino effect of carbon nanotubes”, *Journal of Physics Chemistry. C* 115 20471–20480, 2011.

[63] M. Becton, X. Wang, “Thermal gradients on graphene to drive nanoflake motion”, *Journal of Chemistry Theory and Computation* 10 722–730, 2014.

[64] A. Lohrasebi, M. Neek-Amal, M. Ejtehadi, “Directed motion of C-60 on a graphene sheet subjected to a temperature gradient”, *Physics Review E* 83 042601, 2011.

[65] Z. Guo, T. Chang, X. Guo, H. Gao, “Thermal-induced edge barriers and forces in interlayer interaction of concentric carbon nanotubes”, *Physics Review Letter* 107 105502, 2011.

[66] S. Hernandez, C. Bennett, C. Junkermeier, S. Tsoi, F. Bezares, R. Stine, J. Robinson, E. Lock, D. Boris, B. Pate, J. Caldwell, T. Reinecke, P. Sheehan, S. Walton, “Chemical gradients on graphene to drive droplet motion”, *ACS Nano* 7 4746–4755, 2013.

[67] L. Zhang, X. Wang, “Computational insights of water droplet transport on graphene sheet with chemical density”, *Journal of Applied Physics* 115 194306, 2014.

[68] M. Chaudhury, G. Whitesides, How to make water run uphill, *Science* 256 1539–1541, 1992.

[69] K. Rinne, S. Gekle, D. Bonthuis, R. Netz, Nanoscale pumping of water by ac electric fields, *Nano Letter* 12 1780–1783, 2012.

[70] Y. Wang, Y. Zhao, J. Huang, Giant pumping of single-file water molecules in a carbon nanotube, *Journal of Physics Chemistry B* 115 13275–13279, 2011.

[71] M. Yamamoto, O. Pierre-Louis, J. Huang, M. Fuhrer, T. Einstein, W. Cullen, ‘‘The princess and the pea’’ at the nanoscale: wrinkling and delamination of graphene on nanoparticles, *Physics Review X* 2 041018, 2012.

[72] S. Zhu, T. Li, Wrinkling instability of graphene on substratesupported nanoparticles, *Journal of Applied Mechanics* 061008, 2014.

[73] S. Cranford, D. Sen, M. Buehler, Meso-origami: folding multilayer graphene sheets, *Applied Physics Letter* 95 123121, 2009.

[74] K. Kim, Z. Lee, B. Malone, K. Chan, B. Aleman, W. Regan, W. Gannett, M. Crommie, M. Cohen, A. Zettl, Multiply folded graphene, *Physics Review B* 83 245433, 2011.

[75] J. Qi, J. Huang, J. Feng, D. Shi, J. Li, The possibility of chemically inert, graphene-based all-carbon electronic devices with 0.8 ev gap, *ACS Nano* 5 3475-3482, 2011.

[76] S. Zhu, T. Li, Hydrogenation enabled scrolling of graphene, *Journal of Physics D: Applied Physics* 46 075301, 2013.

[77] S. Zhu, T. Li, Hydrogenation-assisted graphene origami and its application in programmable molecular mass uptake, storage, and release, *ACS Nano* 8 2864-2872, 2014.

[78] D. Yu, F. Liu, Synthesis of carbon nanotubes by rolling up patterned graphene nanoribbons using selective atomic adsorption, *Nano Letters* 7 3046-3050, 2007.

[79] D. Boukhvalov, M. Katsnelson, A. Lichtenstein, Hydrogen on graphene: Electronic structure, total energy, structural distortions and magnetism from first-principles calculations, *Physics Review B* 77 035427, 2008.

[80] D. Elias, R. Nair, T. Mohiuddin, S. Morozov, P. Blake, M. Halsall, A. Ferrari, D. Boukhvalov, M. Katsnelson, A. Geim, K. Novoselov, Control of graphene's properties by reversible hydrogenation: Evidence for graphane, *Science* 323 610-613, 2009.

[81] J. Zhou, Q. Wang, Q. Sun, X. Chen, Y. Kawazoe, P. Jena, Ferromagnetism in semihydrogenated graphene sheet, *Nano Letters* 9 3867-3870, 2009.

[82] N. Levy, S. Burke, K. Meaker, M. Panlasigui, A. Zettl, F. Guinea, A. Neto, M. Crommie, Strain-induced pseudo-magnetic fields greater than 300 tesla in graphene nanobubbles, *Science* 329 544-547, 2010.

[83] K. Kim, Y. Blanter, K. Ahn, Interplay between real and pseudomagnetic field in graphene with strain, *Physics Review B* 84 081401(R), 2011.

[84] F. De Juan, J. Manes, M. Vozmediano, Gauge fields from strain in graphene, *Physics Review B* 87 165131, 2013.

[85] J. Sloan, A. Sanjuan, Z. Wang, C. Horvath, S. Barraza-Lopez, Strain gauge fields for rippled graphene membranes under central mechanical load: An approach beyond first-order continuum elasticity, *Physics Review B* 87 155436, 2013.

[86] N. N. Klimov, S. Jung, S. Zhu, T. Li, C. A. Wright, S. D. Solares, D. B. Newell, N. B. Zhitenev, J. A. Stroscio, Electromechanical properties of graphene drumheads, *Science* 336 1557-1561, 2012.

[87] F. Guinea, M. Katsnelson, A. Geim, Energy gaps and a zero-field quantum hall effect in graphene by strain engineering, *Nature Physics*. 6 30-33, 2010.

[88] S. Zhu, Y. Huang, N. N. Klimov, D. B. Newell, N. B. Zhitenev, J. A. Stroscio, S. D. Solares, T. Li, Pseudomagnetic fields in a locally strained graphene drumhead, *Physics Review B* 90 075426, 2014.

[89] L. Jiang, Y. Huang, H. Jiang, G. Ravichandran, H. Gao, K. Hwang, B. Liu, A cohesive law for carbon nanotube/polymer interfaces based on the van der waals force, *Journal of the Mechanics and Physics of Solids* 54 2436-2452, 2006.

[90] S. Plimpton, Fast parallel algorithms for short-range molecular-dynamics, *Journal of Computation Physics* 117 1-19, 1995.

[91] S. Stuart, A. Tutein, J. Harrison, A reactive potential for hydrocarbons with intermolecular interactions, *Journal of Chemistry Physics* 112 6472, 2000.

[92] Y. Huang, S. Zhu, T. Li, Line defects guided molecular patterning on graphene, *Applied Physics Letters* 104 093102, 2014.

[93] S. Foiles, M. Baskes, M. Daw, Embedded-atom-method functions for the fcc metals cu, ag, au, ni, pd, pt, and their alloys, *Physics Review B* 33 7983, 1986.

[94] S. Arcidiacono, J. Walther, D. Poulikakos, D. Passerone, P. Koumoutsakos, Solidification of gold nanoparticles in carbon nanotubes, *Physics Review Letters* 94 105502, 2005.

[95] W. Xiong, J. Liu, M. Ma, Z. Xu, J. Sheridan, Q. Zheng, Strain engineering water transport in graphene nanochannels, *Physics Reviwe E* 84 056329, 2011.

[96] L. Liu, L. Zhang, Z. Sun, G. Xi, Graphene nanoribbon-guided fluid channel: A fast transporter of nanofluids, *Nanoscale* 4 6279-6283, 2012.

[97] S. Kannam, B. Todd, J. Hansen, P. Daivis, Slip flow in graphene nanochannels, *Journal of Chemistry Physics* 135 144701, 2011.

[98] Y. Qiao, X. Xu, H. Li, Conduction of water molecules through graphene bilayer, *Applied Physics Letters* 103 233106, 2013.

[99] L. Palmer, S. Stupp, Molecular self-assembly into one-dimensional nanostructures, *Accounts of Chemical Research* 41 (12) 1674-1684, 2008.

[100] J. Huie, Guided molecular self-assembly: a review of recent efforts, *Smart Materials and Structures* 12 056329, 2011.

[101] M. Grzelczak, J. Vermant, E. M. Furst, L. M. Liz-Marzan, Direct self-assembly of nanoparticles, *ACS Nano* 4 (7) 3591-3605, 2011.

[102] S. Zhang, Fabrication of novel biomaterials through molecular self-assembly, Nature Biotechnology 21 1171-1178, 2003.

[103] C. D Reddy, Y. W. Zhang, V. B Shenoy, Patterned graphone: a novel template for molecular packing, *Nanotechnology* Volume 23 Number16, 2012.

[104] J. M. Yuk, K. Kim, B. Aleman, W. Regan, J. H. Ryu, J. Park, P. Ercius, H. Lee, A. Alivisatos, M. F. Crommie, J. Lee, A. Zettle Graphene veils and sandwiches, *Nano Letters* 11 (8) 3290-3294, 2011.

[105] L. Tapaszto, G. Dobrik, P. Lambin, L. Biro, Tailoring the atomic structure of graphene nanoribbons by scanning tunneling microscope lithography, *Nature Nanotechnology* **3** 394-401, 2008.

[106] B. S. Gregory, F. Schneider, Q. Xu, G. Pandraud, C. Dekker, H. Zandbergen, Atomic-scale electron-beam sculpting of near-defect-free graphene nanostructures, *Nano Letters* **84** (2011) 056329.

[107] C. D Reddy, Y. W. Zhang, V. B Shenoy, Patterned graphone: a novel template for molecular packing, *Nanotechnology* Volume 23 Number16, 2012.

[108] J. M. Yuk, K. Kim, B. Aleman, W. Regan, J. H. Ryu, J. Park, P. Ercius, H. Lee, A. Alivisatos, M. F. Crommie, J. Lee, A. Zettle, Graphene veils and sandwiches, *Nano Letters* **11** (8) 3290-3294, 2011.

[109] Q. Xu, M. Wu, G. Schneider, L. Houben, S. K. Malladi, C. Dekker, E. Yucelen, R. Dunin-Borkowski, H. W. Zandbergen, Controllable atomic scale patterning of freestanding monolayer graphene at elevated temperature, *ACS Nano* **7** (2) 1566-1572, 2012.

[110] M. Fischbein, M. Drndic, Electron beam nanosculpting of suspended graphene sheets, *Applied Physics Letters* **93**, 113107, 2008.

[111] M. Lemme, D. C. Bell, J. Williams, L. Stern, B.W. Baugher, P. Jarillo-Herrero, C. Marcus, Etching of graphene devices with a helium ion beam, *ACS Nano* **3** (9) 2674-2676, 2009.

[112] G. Compagnini, F. Giannazzo, S. Sonde, V. Raineri, E. Rimini, Ion irradiation and defect formation in single layer graphene, *Carbon* Volume 47 Issue 14 3201-3207, 2009.

[113] S. Plimpton, Fast parallel algorithms for short-range molecular dynamics, *Journal of Computational Physics* Volume 117 Issue 1, 1-19, 1995.

[114] M. Svec, P. Merino, Y. J. Dappe, C. Gonzalez, E. Abad, P. Jelinek, J. A. Martin-Gago, Van der Waals interactions mediating the cohesion of fullerenes on graphene, *Physics Review B* 86 121407 , 2012.

[115] G. Dimitrakakis, E. Tylianakis, G. Froudakis, Pillared graphene: a new 3-D network nanostructure for enhanced hydrogen storage, *Nano Letters* **8** (10), 3166-3170, 2008.

[116] O. Pupysheva, A. Farajian, B.Yakobson, Fullerene nanocage capacity for hydrogen storage, *Nano Letters* **8** (3) 767-774, 2007.

[117] G. Compagnini, F. Giannazzo, S. Sonde, V. Raineri, E. Rimini, Ion irradiation and defect formation in single layer graphene, *Carbon* Volume 47 Issue 14 3201-3207, 2009.

[118] D. Elias *et al.*, Control of graphene's properties by reversible hydrogenation: Evidence for graphane. *Science* **323**, 610-613, 2009.

[119] S. Ryu *et al.*, Reversible basal plane hydrogenation of graphene. *Nano Letters* **8**, 4597-4602, 2008.

[120] X. Wang, S. Tabakman, H. Dai, Atomic layer deposition of metal oxides on pristine and functionalized graphene. *Journal of the American Chemical Society* **130**, 8152–8153, 2008,.

[121] D. Boukhvalov, M. Katsnelson, Chemical functionalization of graphene with defects. *Nano Letters* **8**, 4373-4379, 2008.

[122] D. Boukhvalov, M. Katsnelson, A. Lichtenstein, Hydrogen on graphene: Electronic structure, total energy, structural distortions and magnetism from first-principles calculations. *Physical Review B* **77**, 035427, 2008.

[123] R. Balog *et al.*, Bandgap opening in graphene induced by patterned hydrogen adsorption. *Nature Materials* **9**, 315-319, 2010.

[124] D. Boukhvalov, M. Katsnelson, Chemical functionalization of graphene with defects. *Nano Letters* **8**, 4373-4379, 2008.

[125] D. Boukhvalov, M. Katsnelson, A. Lichtenstein, Hydrogen on graphene: Electronic structure, total energy, structural distortions and magnetism from first-principles calculations. *Physical Review B* **77**, 035427, 2008.

[126] D. Boukhvalov, M. Katsnelson, A. Lichtenstein, Hydrogen on graphene: Electronic structure, total energy, structural distortions and magnetism from first-principles calculations. *Physical Review B* **77**, 035427, 2008.

[127] Z. Sun, C, Pint, D. Marcano, C. Zhang, J. Yao, G. Ruan, Z. Yan, Y. Zhu, R. Hauge, J. Tour, Towards hybrid superlattices in graphene. *Nature Communications* **2**, 559, 2011.

[128] L. Chernozatonskii, P. Sorokin, Nanoengineering structures on graphene with adsorbed hydrogen "lines". *Journal of Physical Chemistry C* **114**, 3225-3229, 2010.

[129] H. Zhang, Y. Miyamoto, A. Rubio, Laser-induced preferential dehydrogenation of graphane. *Physical Review B* **85**, 201409(R) , 2012.

[130] J. Zhou, Q. Sun, How to fabricate a semihydrogenated graphene sheet? A promising strategy explored. *Applied Physics Letters* **101**, 073114 , 2012.

[131] L. Bocquet, P. Tabeling, Physics and technological aspects of nanofluidics. *Lap on a Chip* **14**, 3143-3158, 2014.

[132] H. Park, Y. Jung, Carbon nanofluidics of rapid water transport for energy applications. *Chemical Society Reviews* **43**, 563-576 , 2014.

[133] A. Noy, S. Park, F. Fornasiero, J. Holt, C. Grigoropoulos, O. Bakajin, Nnofluidics in carbon nanotubes. *Nano Today* Volume 2, Issue 6, 22-29, 2007.

[134] M. Walker, R. Weatherup, N. Bell, S. Hofmann, U. Keyser, Free-standing graphene membranes on glass nanopores for ionic current measurements. *Applied Physics Letters* **106**, 023119 , 2015.

[135] Y. Qiao, X. Xu, H. Li, Conduction of water molecules through graphene bilayer. *Applied Physics Letters* **103**, 073114233106 , 2013